Simplified proposal for the temperature field of steel-reinforced CFST columns exposed to fire

David Medall [a], Ana Espinós [a,*], Vicente Albero [b], Manuel L. Romero [a]

[a] *ICITECH, Universitat Politècnica de València, Valencia, Spain*
[b] *Department of Mechanical Engineering and Construction, Universitat Jaume I, Castellón, Spain*

ARTICLE INFO	ABSTRACT
	Concrete-filled steel tubular (CFST) columns are composite sections that may contribute to reduce the environmental impact in construction through a more efficient use of resources. By embedding a steel profile inside a CFST section, a new typology is generated, the so-called steel-reinforced concrete-filled steel tubular (SR-CFST) columns, which may enhance not only the structural capacity of these composite columns at room temperature but also their fire performance. This paper focuses on studying the thermal behaviour of SR-CFST columns under fire conditions, for which purpose a two-dimensional finite element model was developed by the authors and validated by comparing the temperature distribution results with experimental tests available in the literature. Subsequently, parametric studies were carried out to analyse the influence of the relevant parameters – cross-section shape, outer tube thickness, inner steel profile dimensions, section factor – over the cross-sectional capacity of SR-CFST columns exposed to a standard ISO 834 fire. Using the data obtained from the parametric studies, a simplified temperature distribution proposal was derived. In the presented proposal, the composite section was divided onto four components (hollow steel tube, concrete infill, inner steel profile web and flanges) and simplified equations and tables were developed through statistical data processing in order to find the representative equivalent temperature of each part of the section. By doing so, the reduced cross-sectional capacity of a SR-CFST column at a given fire resistance period can be easily evaluated by using a single strength and stiffness value for each component of the section corresponding to its assigned equivalent temperature. This simplified approach may be helpful for practitioners in the fire design process of SR-CFST columns, for which the current provisions in Eurocode 4 Part 1.2 do not provide guidance in predicting the temperature field.

1. Introduction

The premature failure of slender concrete-filled steel tubular (CFST) columns when exposed to fire has been highlighted in previous investigations by the authors [1]. Given these limitations, solutions are sought for improving the fire performance of this typology of composite columns. In recent years, innovative solutions have been developed to increase both the load-bearing capacity and fire resistance of CFST columns [2]. One of these solutions consists of embedding an open steel profile within the concrete infill of the CFST section, generating the so-called steel-reinforced CFST section (SR-CFST), see Fig. 1. In this configuration, the inner steel profile results thermally protected by the surrounding concrete and therefore, its degradation at elevated temperatures is delayed, which may thus help resist the applied load for a more extended period of fire exposure time. This composite section combines the advantages of CFST columns and steel-reinforced concrete (SRC) columns.

Numerous public buildings in China have adopted SR-CFCST columns as the main load-bearing structural members. A successful example of a high-rise building using SR-CFST sections is the Haiyi Hotel in Jiangmen (China), described by Zhou et al. [3].

These types of composite sections are also being gradually introduced in Europe. An example of the use of this solution is the Millennium Tower in Wien (Austria) [4]. It is a fifty-five storey (202 m high) with CFST columns made of outer S355 CHS tubes with a C40–C60 concrete infill. The internal columns of the building have been provided with embedded H profiles to increase their load-bearing capacity. More recent studies covered the use of CFST sections for other innovative applications, such as retaining wall systems [5,6] and massive steel–concrete composite columns and beams [7].

Amongst the scarce experimental investigations found on SR-CFST

Nomenclature

A_i	Cross-sectional area of a cell of the finite element mesh
$A_{a,i}$	Cross-sectional area of a cell of the outer steel tube
$A_{c,i}$	Cross-sectional area of a cell of the concrete infill
$A_{p,i}$	Cross-sectional area of a cell of the inner steel profile
A_m/V	Section factor
B	Outer dimension of the square section
c_p	Specific heat
CES	Concrete encased sections
CFST	Concrete-filled steel tube
D	Outer diameter of the circular section
E_a	Elastic modulus of the steel of the outer tube at room temperature
$E_{a,\theta}$	Elastic modulus of the steel of the outer tube at the temperature θ
$E_{c,sec}$	Secant modulus of concrete at room temperature
$E_{c,sec,\theta}$	Secant modulus of concrete at the temperature θ
E_p	Elastic modulus of the steel of the inner profile at room temperature
$E_{p,\theta}$	Elastic modulus of the steel of the inner profile at the temperature θ
$EI_{y,fi}$	Flexural stiffness of the composite section in the fire situation (minor axis)
$EI_{y,fi,c}$	Flexural stiffness of the concrete infill in the fire situation (minor axis)
$EI_{y,fi,f}$	Flexural stiffness of the steel profile flanges in the fire situation (minor axis)
$EI_{y,fi,w}$	Flexural stiffness of the steel profile web in the fire situation (minor axis)
$EI_{z,fi}$	Flexural stiffness of the composite section in the fire situation (major axis)
$EI_{z,fi,c}$	Flexural stiffness of the concrete infill in the fire situation (major axis)
$EI_{z,fi,f}$	Flexural stiffness of the steel profile flanges in the fire situation (major axis)
$EI_{z,fi,w}$	Flexural stiffness of the steel profile web in the fire situation (major axis)
F	View factor
FE	Finite element
f_c	Compressive cylinder strength of concrete at room temperature
$f_{c,\theta}$	Compressive cylinder strength of concrete at the temperature θ
$f_{y,a}$	Yield strength of the steel of the outer tube at room temperature
$f_{y,a,\theta}$	Yield strength of the steel of the outer tube at the temperature θ
$f_{y,p}$	Yield strength of the steel of the inner profile at room temperature
$f_{y,p,\theta}$	Yield strength of the steel of the inner profile at the temperature θ
h_j	Joint contact conductance
ISCR	Inner Steel Contribution Ratio
$I_{a,i}$	Second moment of area of a cell of the outer steel tube
$I_{c,i}$	Second moment of area of a cell of the concrete infill
$I_{f,i}$	Second moment of area of a cell of the inner steel profile flange
$I_{w,i}$	Second moment of area of a cell of the inner steel profile web
k	Thermal conductivity
$k_{i,\theta}$	Reduction factor for a material property at elevated temperature
$N_{pl,Rd}$	Design cross-sectional plastic resistance to axial compression
$N_{fi,pl,Rd}$	Design cross-sectional plastic resistance to axial compression in fire
$N_{fi,pl,Rd,a}$	Outer steel tube plastic resistance to axial compression in fire
$N_{fi,pl,Rd,c}$	Concrete plastic resistance to axial compression in fire
$N_{fi,pl,Rd,f}$	Steel profile flanges plastic resistance to axial compression in fire
$N_{fi,pl,Rd,w}$	Steel profile web plastic resistance to axial compression in fire
n	Normal direction to a surface
P_m	Perimeter of the exposed surface
q	Heat flux
R	Standard fire exposure time
SR-CFST	Steel-reinforced concrete-filled steel tube
t	Thickness of the outer steel tube
u_s	Concrete cover
y_i	Coordinate of the centroid of a cell of the FE mesh (perpendicular to major axis)
z_i	Coordinate of the centroid of a cell of the FE mesh (perpendicular to minor axis)
α_c	Convective coefficient
ε	Emissivity
ε_{cu}	Concrete strain at room temperature
$\varepsilon_{cu,\theta}$	Concrete strain at the temperature θ
θ	Temperature
θ_i	Temperature of the centroid of a cell of the FE mesh
θ_a	Temperature of the outer steel tube surface
$\theta_{a,eq}$	Equivalent temperature of the outer steel tube
$\theta_{c,eq}$	Equivalent temperature of the concrete infill
$\theta_{f,eq}$	Equivalent temperature of the flanges of the inner steel profile
$\theta_{w,eq}$	Equivalent temperature of the web of the inner steel profile
θ_g	Gas temperature in the vicinity of the fire exposed member
θ_m	Surface temperature of the exposed member
θ_r	Effective radiation temperature of the fire environment
θ_{exp}	Experimentally measured temperature
θ_{num}	Numerically calculated temperature
ρ	Density
σ	Stephan-Boltzmann constant

columns exposed to fire conditions, the works from Chu et al. [8–10], Zhu et al. [11] and Meng et al. [12] can be cited. The first authors tested at elevated temperature ten columns filled with self-compacting concrete embedding another steel profile. Four of the column specimens used an embedded HEB profile - two of which were protected by intumescent coating- and were tested with time resistance times ranging between 39 and 79 min. The experimental results were completed through a numerical model developed by the authors using the SAFIR computer code. Regarding the studies by Zhu et al. [11], eight fire resistance tests were carried out on SR-CFST columns filled with normal strength concrete under non-uniform fire conditions. Five square and three circular SR-CFST columns were tested. More details of these fire tests can be found in [13] for the square SR-CFST sections and [14] for the circular SR-CFST sections. In the same research framework, Meng et al. [12] studied experimentally the residual strength of SR-CFST stub columns after exposure to iSO-834 fire. Three square SR-CFST columns composed of an outer SHS and an inner steel profile were exposed from 2, 3 and 4 sides inside a small electric furnace. Once cooled down, the column specimens were loaded incrementally until failure to obtain their residual strength. Based on the results of parametric studies

conducted by the authors, formulae were proposed for predicting the residual strength of SR-CFST columns after different types of fire exposure.

In light of the review of the experimental programmes published in the literature, it can be seen that the number of available fire test results on SR-CFST columns is still scarce. Given the lack of sufficient experimental evidence, researchers worldwide have focused on studying the fire performance of SR-CFST sections through analytical or numerical models.

The first work which can be found in the literature on the analytical resolution of the transient heat conduction in concrete filled steel hollow sections exposed to fire is that from Lie [15]. Based on the finite differences method [16], Lie and co-workers derived expressions which allow to calculate the temperature of the concrete core and steel tube by subdividing the cross-sectional area of the column in a number of layers for CHS columns [17,18] or elements in the case of RHS columns [19].

Later investigations by Tan & Tang [20] extended the Rankine method to the analyses of plain and reinforced concrete filled tubular columns at elevated temperatures.

Wang & Tan [21] presented a theoretical approach for the heat transfer analysis of concrete filled steel circular hollow sections subjected to fire based on an analytical Green's function solution. This approach can be used to predict the temperature field inside the composite domain and the heat flux at the fire and steel–concrete interfaces.

Despite the analytical solution of CFST sections with different geometries (circular, square) has been widely covered by researchers in the last decades, when it comes to SR-CFST sections, the multiple steel–concrete interfaces and the complex thermal gradient generated within the inner profile make it difficult to derive analytical equations, reason that has motivated researchers to the development of numerical models that facilitate this task.

The numerical investigation conducted by Espinós et al. [22] compared the fire performance of different types of innovative steel–concrete composite columns – SR-CFST columns among them – and proposed strategies for enhancing the fire resistance of traditional CFST columns by using inner steel profiles. The numerical model was developed in ABAQUS using three-dimensional eight-noded solid elements for the steel tube and concrete core and four-noded three-dimensional bilinear rigid quadrilateral elements with a maximum finite element size of 20 mm. The thermal resistance at the steel–concrete interface was assumed via a constant value for the gap conductance parameter. The error obtained with this model (test/prediction) was 1.08 with a standard deviation equal to 0.19. It was observed that by "splitting" the outer steel tube into two profiles and moving most of the amount of steel towards the inner part of the section, the resisting profile resulted "internally" protected by the surrounding concrete. Thus its degradation at elevated temperatures was delayed, lengthening the fire endurance of the column. It was also found that the fire performance of SR-CFST columns might be significantly enhanced by using high strength steel at the inner profiles.

Tan et al. [23,24] developed a numerical model for SR-CFST columns using stainless steel at the outer tube. These authors carried out additional parametric studies in order to assess and optimise the performance of these composite sections and quantify the increase in terms of fire resistance when introducing an inner steel profile in CFST sections with carbon steel or stainless-steel outer tube. The model was meshed setting a maximum finite element size of 20 mm. Solid elements were used for the in-filled concrete, while shell elements were used for the steel tube and profile. The model had a mean error value of 1.048 and a coefficient of variation of 0.071 for the circular columns and 1.055 and 0.072 respectively for the square columns. It was found that the SR-CFST columns with stainless steel outer tube exhibited an enhanced fire resistance over the corresponding CFST and CFSST columns with the same cross-sectional area or load-bearing capacity at room temperature.

Mao et al. [25] presented a numerical study on the fire performance of SR-CFST columns with square cross-sections. The influence of parameters such as the column slenderness, concrete and steel strength and the steel ratio of the outer tube and inner profile were assessed through numerical simulations. The mesh of the model used in this study employed 8-node brick elements (DC3D8) for all components and a maximum finite element size of 20 mm. A constant value of 0.01 $m^2 \, {}^\circ C/W$ was assumed for the thermal resistance at the steel–concrete interface. The mean value and standard deviation values obtained were 1.083 and 0.076 respectively. It was found that the proportions of the steel used at the outer tube and inner profile have a notable influence on the fire resistance of SR-CFST columns. The authors also highlighted the potential of using high strength steel at the inner profile for enhancing the fire resistance, which was in line with the findings by Espinós et al. [22].

A finite element model for SR-CFST columns subjected to non-uniform fire was developed by Meng et al. [13,14] and validated against the tests previously reported in Zhu et al. [11]. Four-noded shell elements, S4R, were used in this study. The interaction between the outer steel tube and the inner concrete core was introduced via a constant value of 200 W/m^2 for the gap conductance. An average ratio of experimental ultimate bearing capacity N_{cr} to the simulated results N'_{cr} was 0.98 and the standard deviation was 0.015. Parametric studies were carried out employing the numerical model in order to assess the application of the existing fire design methods of CFST columns to SR-CFST columns. Regarding the design guidance, at present, there is no specific method in the literature or international design codes that cover this type of sections. In the absence of a specific calculation method, the fire design approach for CFST sections developed by the authors of this paper in previous investigations [26] – which is currently used in Europe
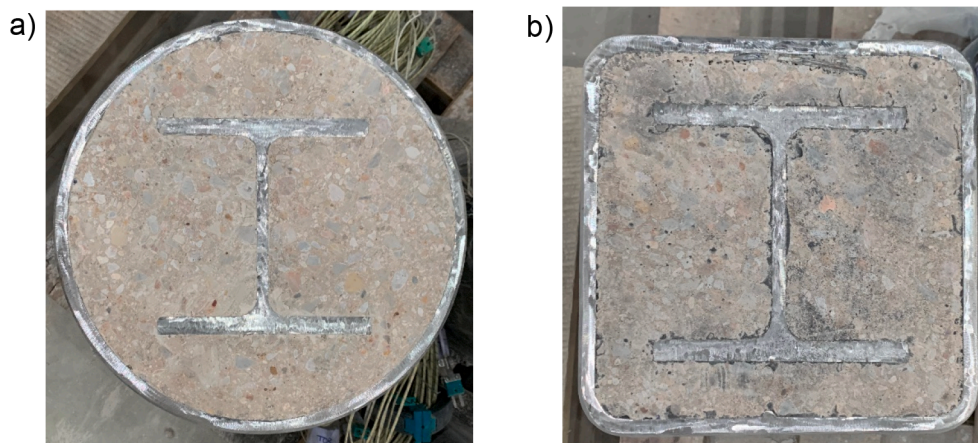

Fig. 1. SR-CFST sections studied in this paper: (a) circular; (b) square.

in replacement of the Annex H method of EN1994-1-2 – was tentatively applied to SR-CFST columns. The method produced conservative results in predicting the fire resistance of axially loaded SR-CFST columns under uniform fire exposure conditions. However, it was concluded that further research is needed to provide accurate predictions for different types of loading (i.e. eccentricities) and fire exposure conditions (i.e. non-uniform fire). It should be pointed out that, since SR-CFST sections are beyond the scope of the new Annex H method, fixed "equivalent" values for in certain parameters (i.e. reinforcement ratio and member slenderness) were assumed by Meng et al. as an intend to apply the method to SR-CFST sections, assimilating the inner steel profile of the SR-CFST section to a reinforcement in a CFST section. This may be a possible source of the deviations found in the predictions; therefore, further research is needed to develop a specific design method for the fire evaluation of SR-CFST columns.

In light of the revision of state of the art, where the scarce number of investigations available on SR-CFST sections has been evidenced, as well as the lack of guidance in Eurocode 4 Part 1.2 [27] for this type of sections, it can be seen that there is a need for developing design equations that allow predicting the temperature distribution in SR-CFST sections in order to evaluate the axial capacity of the columns when subjected to fire. This will be one of the aims of this paper, where a finite element thermal model will be developed and generalized through parametric studies to develop a simplified design proposal that will provide practitioners with a practical tool to easily predict the cross-sectional capacity of SR-CFST sections under fire conditions.

2. Development of the finite element model

A two-dimensional (2D) finite element model was developed utilizing the general-purpose nonlinear finite element analysis package ABAQUS [28]. As this research focuses on the thermal behaviour of SR-CFST columns exposed to a standard fire, a 2D model is enough to analyse the temperature development within the section, assuming that the columns are uniformly exposed in all their length. The use of a 2D model is suitable in this scenario, since the primary goal of the numerical model is to evaluate the cross-sectional plastic resistance and flexural stiffness values at the critical section of the columns. This decision may provide conservative results in the case of a non-uniform fire exposure. Moreover, as this thermal model does not take into account the situation of localized fires but a generalized fire at the compartment (post-flash-over), the assumption of considering the column uniformly exposed along its full length can be made. The main characteristics of the developed numerical model are described in the following subsections.

2.1. Geometry and finite element mesh

The geometry of the model is composed of an assembly of three different parts: outer steel tube, concrete encasement and inner steel profile.

These parts are meshed using 3-node linear heat transfer triangles (DC2D3) with nodal temperature degree of freedom. Based on the results of a mesh sensitivity study (see the following subsection), a maximum finite element (FE) size of 10 mm was used. An example of the FE mesh for a circular SR-CFST section can be seen in Fig. 2.

2.1.1. Mesh sensitivity study

A mesh sensitivity study was performed to select the optimal size of the finite elements in the thermal model. Three different FE sizes were considered: 5, 10 and 20 mm.

Specimens 3A and 4A tested by Chu et al. [8–10] were numerically simulated to evaluate the appropriate mesh density. As shown in Fig. 3, a coarser mesh (20 mm FE) produced considerable deviations when comparing the numerically predicted temperatures with the measured temperatures at the selected thermocouple locations. In turn, FE sizes of 5 and 10 mm provided more accurate predictions in terms of
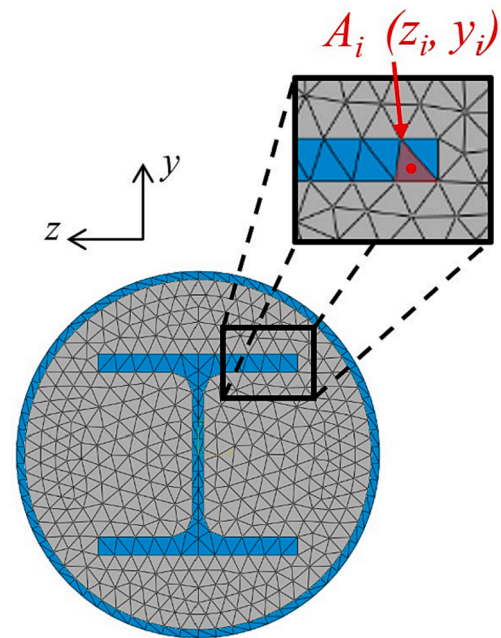

Fig. 2. Detail of the centroid position (z_i, y_i) and area (A_i) of a given triangular i-element of the mesh.
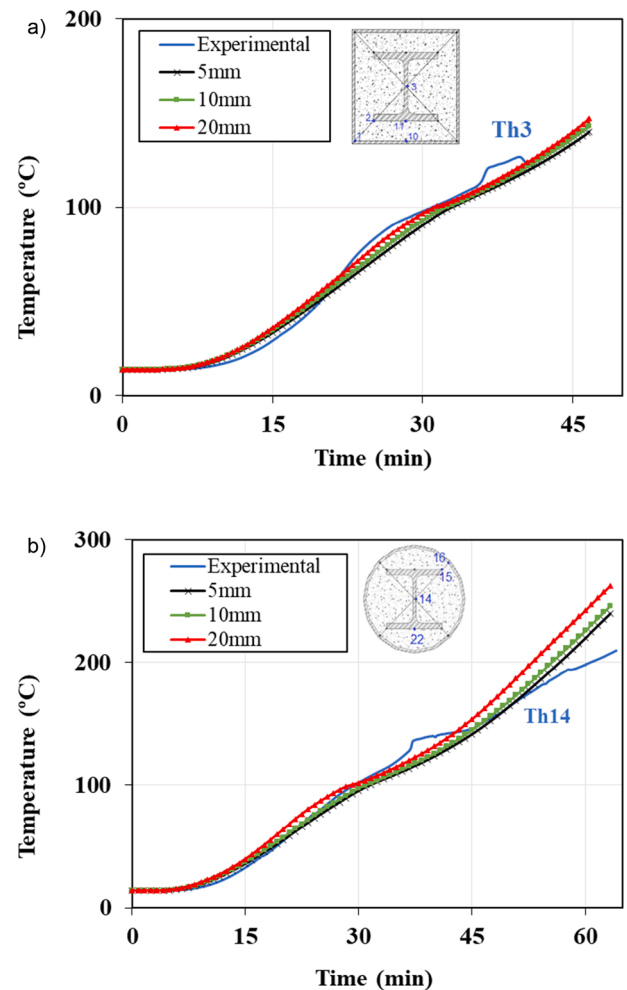

Fig. 3. Mesh sensitivity analysis. Comparison with the case specimens tested Chu et al. [5]: (a) 3A, (b) 4A.

temperature, being relatively close to the experimental results. Given the similarity in the temperature predictions obtained with 5 and 10 mm, the second FE size (10 mm) was chosen, as a more refined mesh (5 mm) does not result in a greater precision while it would lead to a higher computational cost.

Therefore, the suitable element size which provided accurate results with reasonable computational times was found to be 10 mm for the sectional dimensions covered in this paper.

2.2. Thermal analysis and boundary conditions

A nonlinear heat transfer analysis was conducted in ABAQUS for computing the temperature field of the studied SR-CFST sections subjected to fire conditions. The heat balance equation given in (1), based on the Fourier's law of heat conduction, was implemented in the numerical model. The fire action was applied in the model to the exposed surface of the SR-CFST section as a thermal load through the convection and radiation heat transfer mechanisms, which are driven by the equations given in (2).

$$\nabla(\boldsymbol{k} \bullet \nabla \theta) = \rho c_p \frac{\partial \theta}{\partial t} \tag{1}$$

$$-\boldsymbol{n} \bullet \boldsymbol{k} \bullet \nabla \theta = \alpha_c (\theta_m - \theta_g) + F \bullet \varepsilon \bullet \sigma \left(\theta_r^4 - \theta_g^4 \right) \tag{2}$$

where θ_m is the surface temperature of the exposed member and θ_g and θ_r are the gas temperature in the vicinity of the fire exposed member and the effective radiation temperature of the fire environment, respectively.

The evolution of the fire temperature in the model was assumed to follow the standard iSO-834 curve, for the cases analysed in the parametric studies. In those cases used for validation, where the temperature history of the real fire curve applied at the test was known, the average temperature–time curve measured inside the furnace was used, since this can be an important source of error when validating the model.

The values recommended in EN 1991-1-2 [29] were adopted for the governing parameters of the heat transfer problem. For the heat transfer portion by convection, a convective coefficient $\alpha_c = 25$ W/m^{2}K was assumed at the exposed steel surface.

For the radiative portion of heat transfer, an emissivity value $\varepsilon = 0.7$ was adopted at the exposed steel surface, while the emissivity of the fire was taken as $\varepsilon = 1$ and the Stephan-Boltzmann constant $\sigma = 5.67 \cdot 10^{-8}$ W/m^{2}K^4.

The nonlinear heat transfer analysis results consisted of the time evolution of the nodal temperatures (NT11) at the different nodes of the FE mesh. For example, Fig. 4 shows a plot of the numerically predicted cross-sectional temperature field for specimens 3A and 4A tested by Chu et al. [9] at two standard fire periods (30 and 60 min).

2.3. Steel-concrete interface

When exposed to elevated temperatures, the outer steel tube separates transversely from the concrete infill due to the different thermal expansion coefficients of steel and concrete. This phenomenon causes the opening of physical space at the interface between the steel tube and
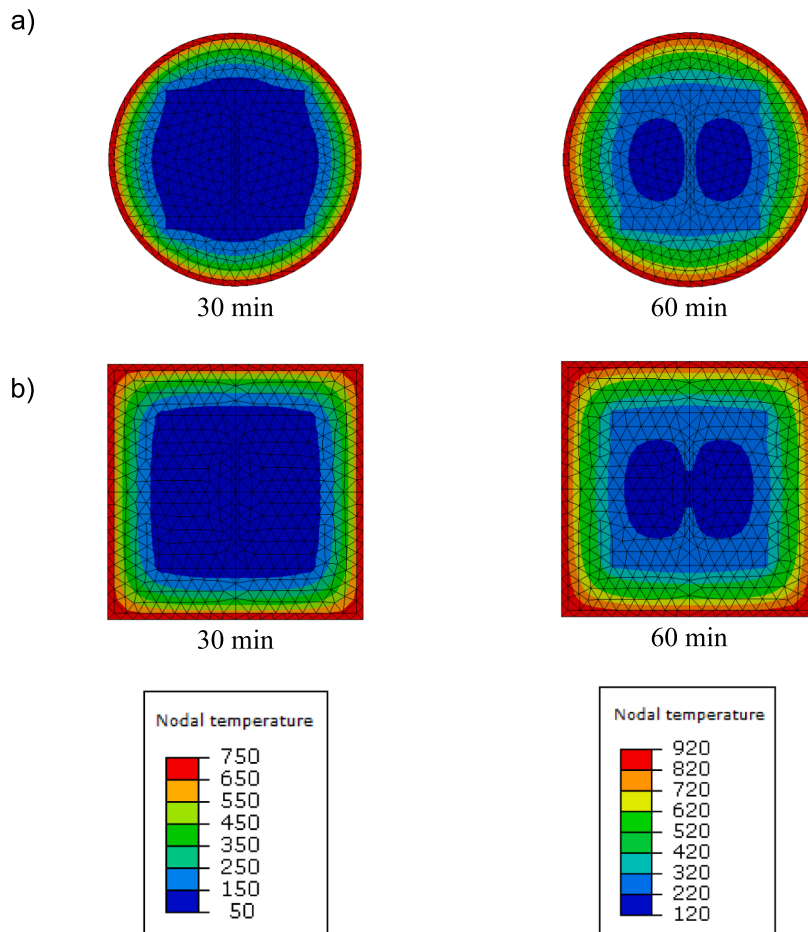

Fig. 4. Temperature field of the SR-CFST sections tested by Chu et al. [5] obtained from the numerical simulations: (a) 3A, (b) 4A.

the concrete infill, which can be considered an "air gap".

This resistance to heat flow is known as the contact thermal resistance and is usually expressed in terms of a joint contact conductance (h_j), defined as:

$$q = h_j \bullet \Delta\theta \tag{3}$$

where $\Delta\theta$ is the temperature difference between the two contacting surfaces at the interface.

The effect of this "air gap" in CFST sections was studied by Ghojel [30], proving that this effect causes a thermal resistance at the boundary between steel and concrete and thus a temperature difference between the outer steel tube and the concrete core. Based on experimental measurements, Ghojel proposed an expression for estimating the interface thermal conductance in circular and square CFST sections as a function of the temperature:

$$h_j = 160.5 - 63.8 \bullet \exp\left(-339.9 \bullet \theta_a^{-1.4}\right) W/m^2 \bullet K \tag{4}$$

where θ_a is the temperature of the outer steel tube surface in degrees Celsius.

Tao and Ghannam [31] proposed a new expression to evaluate the thermal contact conductance, as a function of the sectional dimensions:

$$\text{Circular columns}: \; h_j = 516 \bullet (D/100)^{-2.373} W/m^2 \bullet K \tag{5}$$

$$\text{Square/rectangular columns}: \; h_j = 115 \bullet (B/100)^{-0.85} W/m^2 \bullet K \tag{6}$$

where D is the diameter of the circular tube and B is the side length of a square or rectangular tube (in mm).

This model tends to stabilise around a constant value for massive sections (over 300 mm outer dimension), equal to 38.1 W/m²K for circular columns and 45.2 W/m²K for rectangular columns. Therefore, the influence of the outer dimension in the contact conductance value predicted by this model is more noticeable for reduced sectional dimensions, more pronounced for circular sections.

The described thermal resistance at the boundary between the outer steel tube and the concrete encasement was considered in the numerical model through the "gap conductance" option in ABAQUS [28]. Based on the sensitivity study results (presented in the following sub-section), a constant gap conductance value of 200 W/m²K was used to model the thermal resistance at this interface.

However, for modelling the thermal contact between the concrete infill and the inner steel profile, a "perfect thermal contact" was considered – i.e., the temperatures of the steel profile and concrete are coupled at the interface – due to the reduced temperatures that can be reached at the inner parts of the composite section, no transversal separation is expected between the profile and the surrounding concrete encasement. Therefore, these surfaces are considered to remain in perfect contact during all the fire exposure. Other researchers already used this assumption with enough accuracy [24,25].

2.3.1. Sensitivity analysis for the gap conductance model at the outer steel tube-concrete interface

Three different options for modelling the "gap conductance" at the interface between the outer steel tube and the concrete core were studied. On a first assumption, a constant value of $h_j = 200$ W/m²K was employed, as used by the authors in previous investigations [32]. The second option considered the gap conductance model as a function of the steel temperature suggested by Ghojel [18]. The third option used the model by Tao and Ghannam [31], dependent on the outer sectional dimensions.

The sensitivity analysis results on the gap conductance value can be seen in Fig. 5, where the prediction of temperatures at different points of the section are compared with the measured temperatures under the three models studied. As it can be seen, the computed temperatures at the outer steel tube are similar under the three models. However, at the monitored point of the concrete infill – located close to the interface -the
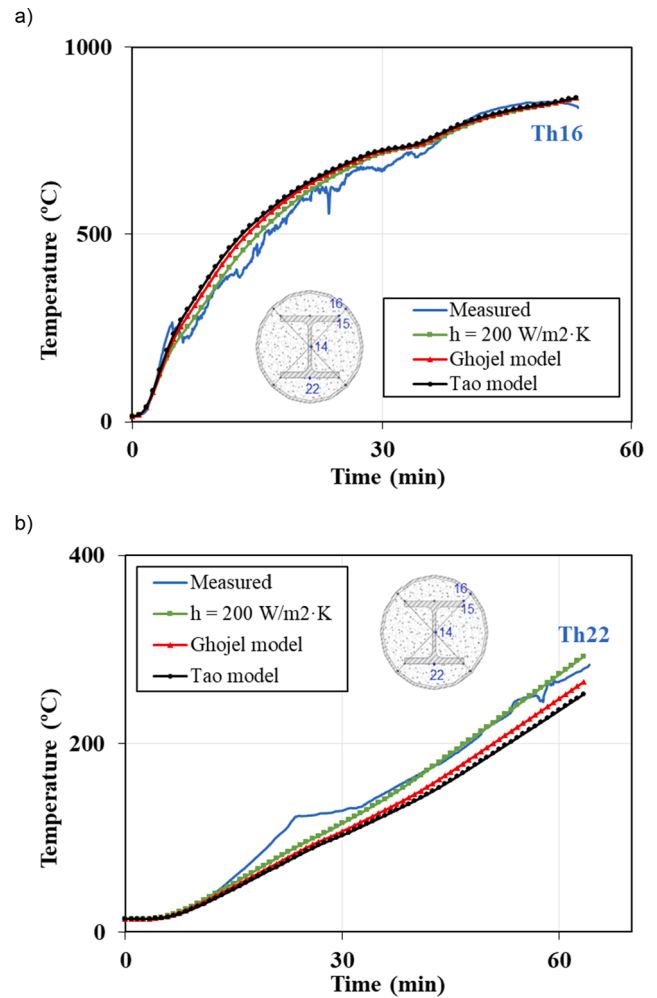
Fig. 5. Sensitivity analysis on the "gap conductance" model. Comparison with case 3A tested by Chu et al. [5].

best prediction was obtained assuming a constant gap conductance value. This observation was similar for other case specimens used to validate the numerical model from the tests available in the literature, although these results have not been included here for extension reasons.

It is worth noting that the model from Ghojel [30], dependent on the temperature of the outer steel tube is more time consuming, as it requires updating the gap conductance value at each calculation step as the temperature of the steel tube increases during the fire exposure. Therefore, assuming a constant value of $h_j = 200$ W/m²K does not mean a loss of accuracy, while it allows for a more economical computing strategy in view of the parametric studies to be carried out in the framework of this research.

2.4. Material properties at elevated temperatures

The temperature-dependent thermal properties of the materials were accounted for in the numerical model.

For steel, the temperature-dependent thermal properties – specific heat (c_p) and thermal conductivity (k) – given in EN 1993-1-2 [33] were adopted.

The thermal properties for concrete at elevated temperatures were obtained from EN 1992-1-2 [34]. However, for modelling the thermal conductivity (k), the new model proposed in the draft version of prEN 1992-1-2:2021 [35] was adopted, which recommends using a transition between the upper and lower limit in the range of temperatures between

140 and 160 °C.

The latent heat of water vaporisation was taken into account through a peak value in the specific heat (c_p) formulation of concrete between 100 and 200 °C, as per Clause 3.3.2(8) in EN 1994-1-2 [27]. When no test data was available, a moisture content equal to 4 % of the concrete weight was assumed in the numerical model by default, as recommended in Clause 3.3.2(7) of EN 1994-1-2 [27], which was modelled through a peak value of 5577.9 J/Kg·K in the specific heat formulation.

3. Validation of the thermal model

In this section, the described numerical model is validated by comparing the temperature distribution results with experimental tests on SR-CFST columns available in the literature.

3.1. Validation of the thermal response of steel-reinforced CFST sections

The main characteristics of the SR-CFST case specimens used for validation are given in Table 1.

In the first validation stage, the experimental results from Chu et al. [9] were used. Specimens 3A and 4A were selected from the reported tests, the former consisted of a circular hollow steel tube of 219.1 × 5 mm with an embedded HEB 120 profile and the latter was a square hollow steel tube of 200 × 5 mm with the same embedded profile. A 6 % moisture value was considered, as reported in the experimental campaign, which equals to a specific heat peak value of 8518.6 J/Kg·K.

Tests 3B and 4B, protected with intumescent paint, were also tentatively compared for extending the validation, although fire-protected sections are out of the scope of this research.

The results of comparing the temperature evolution at the relevant points between the numerical simulations and the experimental thermocouple measurements reported by Chu et al. [9] can be seen in Fig. 6.

Additionally, four square and two circular SR-CFST sections from the experimental programme carried out by Zhu et al. [11] were numerically simulated. The cross-sectional dimensions of the outer square hollow sections (specimens S1H, S2H, S3H and S4H) were 300 mm × 300 mm × 6 mm, while the dimensions of the outer circular hollow sections (specimens C2H and C4H) were 300 mm × 8 mm. The inner steel profile was, in all cases, an H-section HW 150 × 150 (150 mm × 150 mm × 7 mm × 10 mm) according to the Chinese standard GB706-2008. The actual non-uniform fire exposure conditions of these tests
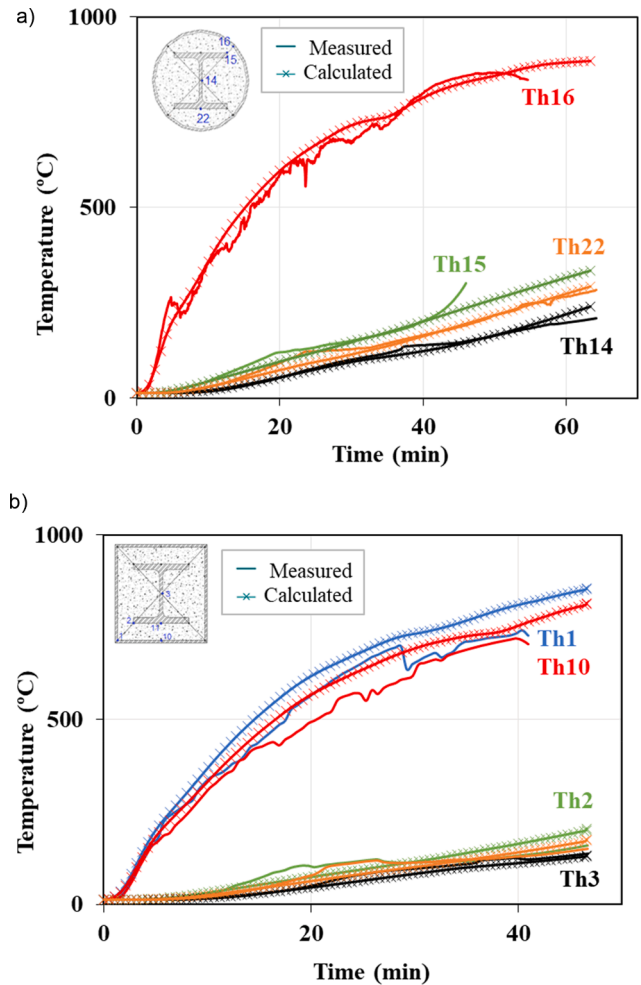

Fig. 6. Comparison between measured and computed temperature–time curves for the case specimens tested Chu et al. [5]: (a) 3A, (b) 4A.

Table 1
Summary of the geometrical and material properties of the column specimens used for validation.

Specimen	D (mm) B (mm)	t (mm)	$f_{y,tube}$ (MPa)	Inner profile	$f_{y,profile}$ (MPa)	f_c (MPa)	Exposure type	Fire protection	Moisture
SR-CFST sections									
3A [5]	219.1	5	420	HEB120	375	35	4-side	–	6 %
3B [5]	219.1	5	420	HEB120	375	35	4-side	Intumescent coating	6 %
4A [5]	200	5	510	HEB120	375	35	4-side	–	6 %
4B [5]	200	5	510	HEB120	375	35	4-side	Intumescent coating	6 %
C4H [7]	300	8	360	HW 150 × 150	345	55	4-side	–	5 %
C2H [7]	300	8	360	HW 150 × 150	345	55	½-section	–	5 %
S4H [7]	300	6	360	HW 150 × 150	345	55	4-side	–	5 %
S3H [7]	300	6	360	HW 150 × 150	345	55	3-side	–	5 %
S2H [7]	300	6	360	HW 150 × 150	345	55	2-side	–	5 %
S1H [7]	300	6	360	HW 150 × 150	345	55	1-side	–	5 %
CES sections									
RCC03 [25]	300 × 300			UC152 × 152 × 37	320	43	460	4-side	4 %
SZCC03 [20]	350 × 350			UC254 × 254 × 73	320	44	460	4-side	4 %
SZCC04 [20]	400 × 400			UC305 × 305 × 97	400	44	460	4-side	4 %
FR4S06 [21]	300 × 300			175 × 175 × 7.5 × 11	242.3–281.3	40	335	4-side	5.79 %
FR4S38 [21]	350 × 250			200 × 150 × 6 × 9	242.3–281.3	40	335	4-side	5.79 %
FR3S37 [21]	350 × 250			200 × 150 × 6 × 9	242.3–281.3	40	335	3-side	5.79 %
FR3S65 [21]	350 × 250			200 × 150 × 6 × 9	242.3–281.3	40	335	3-side	5.79 %
SRC1-1 [22]	300 × 300			150 × 150 × 10 × 10	307	38	383	4-side	4 %
SRHSC-1 [29]	300 × 300			200 × 200 × 8 × 12	380	121.1[a]	504	4-side	< 3 %

[a] Ultra-high-strength concrete with 0.5% steel fibers and 0.15% polypropylene fibers in volume.

were reproduced by the numerical model, with some of the columns being subjected to one, two, three or four-side fire exposure. Ceramic fibre blankets with thermal conductivity of 0.1–0.2 W/m°C were used for materialising the thermal insulation of the specimens subjected to non-uniform fire exposure. A 5 % moisture value was considered for simulating these case specimens, which was introduced via a specific heat peak value of 7048.2 J/Kg·K, as reported in the experimental campaign.

The results of comparing temperatures between the numerical model and the experimental test reported by Zhu et al. [11] are given in Fig. 7.

3.2. Validation of the thermal response of concrete-encased sections

Given the lack of sufficient experimental evidence on the thermal behaviour of SR-CFST sections, the validation of the numerical model was complemented by comparison with experimental test results of Concrete Encased Sections (CES) subjected to elevated temperatures. These sections consist of a reinforced concrete section with an embedded open steel profile; therefore, the information on the temperature field results helpful in verifying the thermal response of the numerical model, with the only particularity of the absence of the outer steel tube. A summary of the main characteristics of the CES sections used in this complementary validation is given in Table 1.

The tested specimens for validation of CES sections were taken from the experimental campaigns carried out by Huang et al. [36,37], Mao & Kodur [38], Han et al. [39] and Du et al. [40].

Test RCC03 was selected from Huang et al. [36], consisting of a square section of dimensions 300 × 300 mm. In turn, tests SZCC03 and SZCC04 were taken from Huang et al. [26], with outer dimensions 350 × 350 mm and 400 × 400 mm, respectively, to extend the validation to a wide range of sectional dimensions. In the absence of test data on the measured moisture content of these experimental programmes, a value of 4 % was considered. The results of comparing the numerical simulations with the cases tested by Huang et al. are given in Fig. 8 (test RCC03) and Fig. 9 (tests SZCC03, SZCC04).

Additionally, four test specimens from Mao & Kodur [38] were considered, as given in Table 1. These cases included three rectangular sections of dimensions 350 × 250 mm and one square section of 300 × 300 mm. The average moisture content at the time of the fire test (120 days) reported by the authors was considered in the numerical simulations, with a value of 5.79 %. This was modelled by a peak value of 8209.8 J/Kg·K in the specific heat formulation. The comparison of the temperature evolution at the relevant points of the section for two of the analysed specimens (FR4S06 and FR4S38) can be seen in Fig. 10.

Case specimen SRC1-1 from Han et al. [39] was used in this validation, consisting of a square section of dimensions 300 × 300 mm. Again, in the absence of test data on the measured moisture content of these experimental programmes, a value of 4 % was considered. The comparison of the evolution of temperatures between the numerical simulation and test for this case specimen can be seen in Fig. 11.

Finally, the validation was completed with one particular test specimen from Du et al. [40], made of ultra-high-strength concrete. Steel fibres with a dosage of 0.5 % in volume were added to the concrete mix to improve its ductility, while 0.15 % of polypropylene fibres were added to prevent spalling at elevated temperatures. The moisture content of concrete was measured during the tests, lower than 3 %, which was introduced by a specific heat peak value of 4107.5 J/Kg·K. The temperature evolution can be seen in Fig. 12.

3.3. Summary of the validation

A summary of the validation of the numerical model is presented in Fig. 13, where for each case specimen used for validation, the predicted and measured temperatures at the location of the thermocouples are plotted for different fire exposure times (30, 60, 90, 120 min). A good agreement is observed, with most points within the ±15 % boundaries.

The mean and standard deviation values of the temperature predictions have been summarised in Table 2, where the prediction errors have been calculated as $\theta_{num}/\theta_{exp}$, a mean value higher than 1 meaning that the thermal model is conservative (i.e., higher temperature predicted by the numerical model in comparison with the experimental
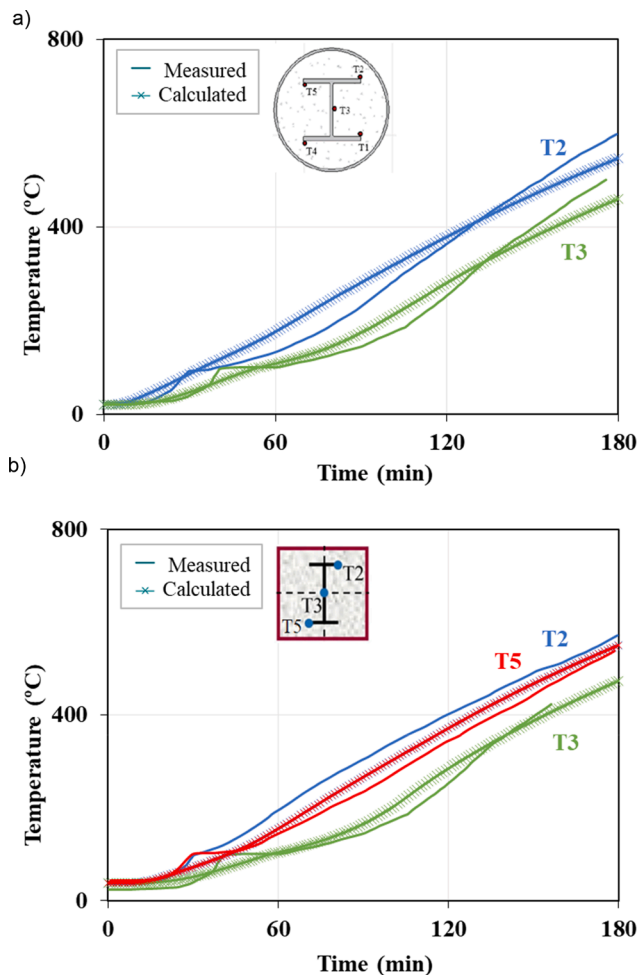

Fig. 7. Comparison between measured and computed temperature–time curves for the case specimens tested by Zhu et al. [7]: (a) C4H, (b) S4H.
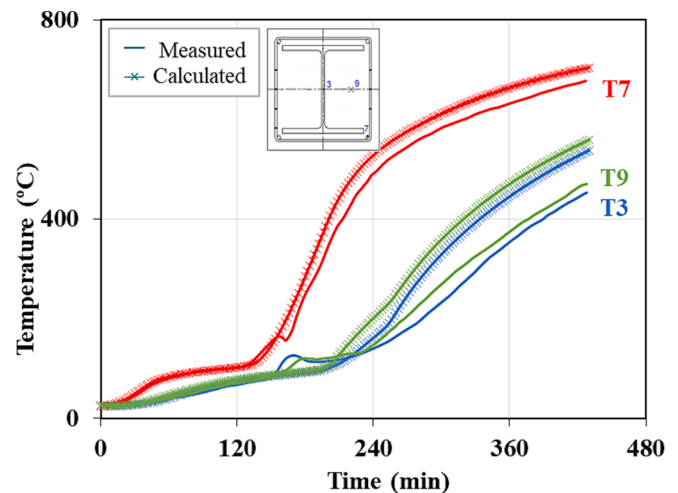

Fig. 8. Comparison between measured and computed temperature–time curves at the relevant points of the section for case RCC03 from Huang et al. [25].
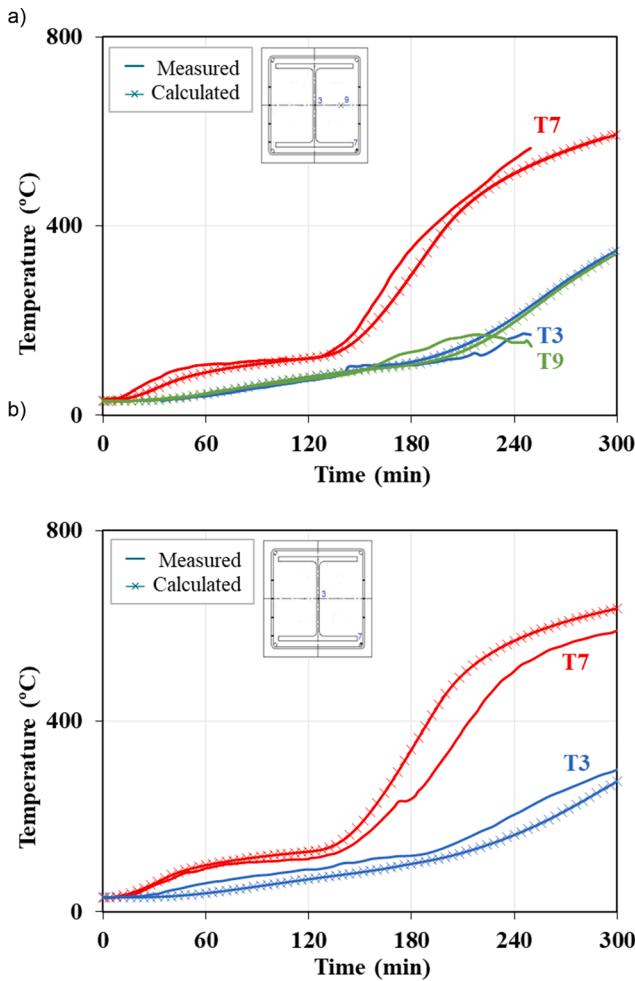
Fig. 9. Comparison between measured and computed temperature–time curves for the case specimens from Huang et al. [26]: (a) SZCC03, (b) SZCC04.

Fig. 10. Comparison between measured and computed temperature–time curves for the case specimens from Mao & Kodur [27]: (a) FR4S06, (b) FR4S38.

Fig. 11. Comparison between numerical and experimental temperature–time curves at the relevant points of the section for case SRC1-1 from Han et al. [28].

value). The average value of the prediction errors accounting for all the columns analysed is 1.03 with a standard deviation of 0.20. Thus, the model can be considered accurate and slightly conservative. It can also be seen in Table 2 that the thermal model predictions are more accurate for temperatures higher than 300 °C, with an average value of 0.99 and a narrower dispersion (0.08 standard deviation). The reason is that in the range of temperatures between 100 °C and 200 °C, the evaporation of the moisture content in concrete occurs, which produces a plateau in the temperature–time curves that is difficult to predict by the numerical model. It is worth reminding that the water vaporisation in concrete has been implicitly accounted for through the specific heat formulation, which causes this deviation at low temperatures. However, when the evaporation phenomena finish and the concrete temperature skips this plateau, the model can predict the evolution of temperatures with reasonable accuracy.

In view of this comparison, and given the variety of sections studied, the different experimental sources compared, and the lack of further details on parameters such as the concrete moisture content, the accuracy of the temperature predictions is considered appropriate. Therefore, the numerical model is judged reliable for conducting parametric studies on the thermal behaviour of SR-CFST sections, which will be carried out in the following section.
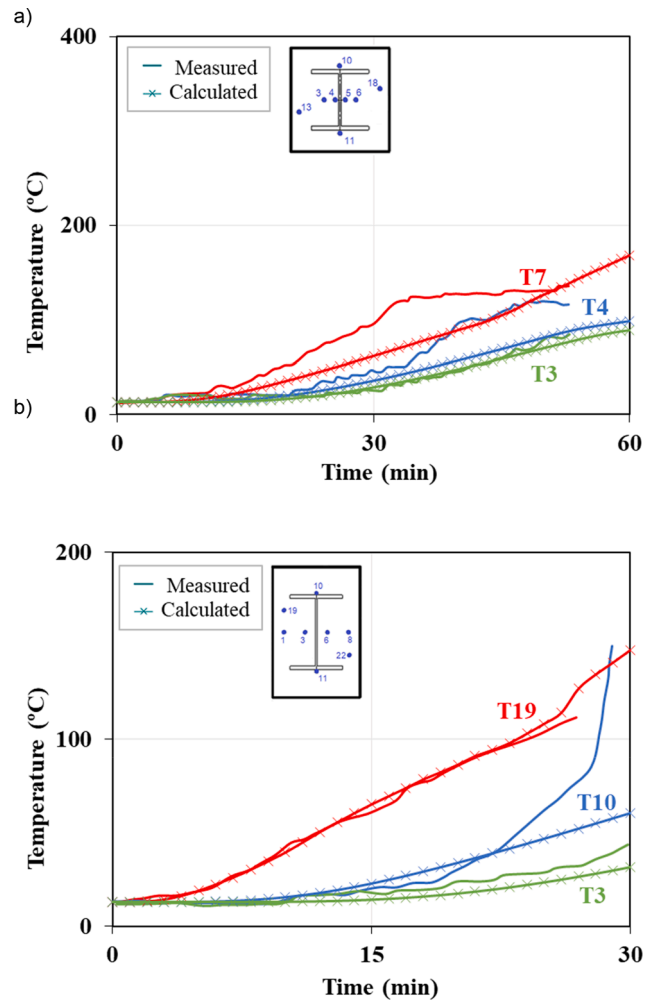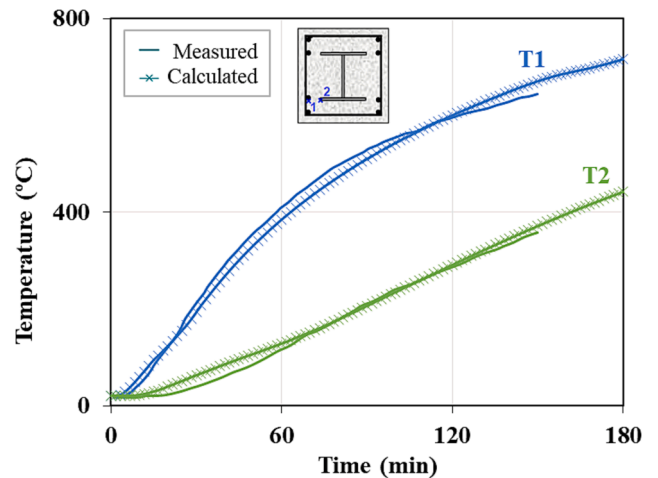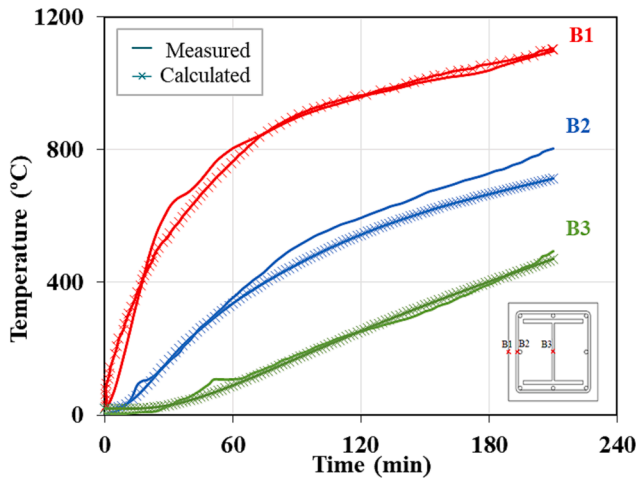
Fig. 12. Comparison between numerical and experimental temperature–time curves at the relevant points of the section for case SRHSC-1 from Du et al. [29].
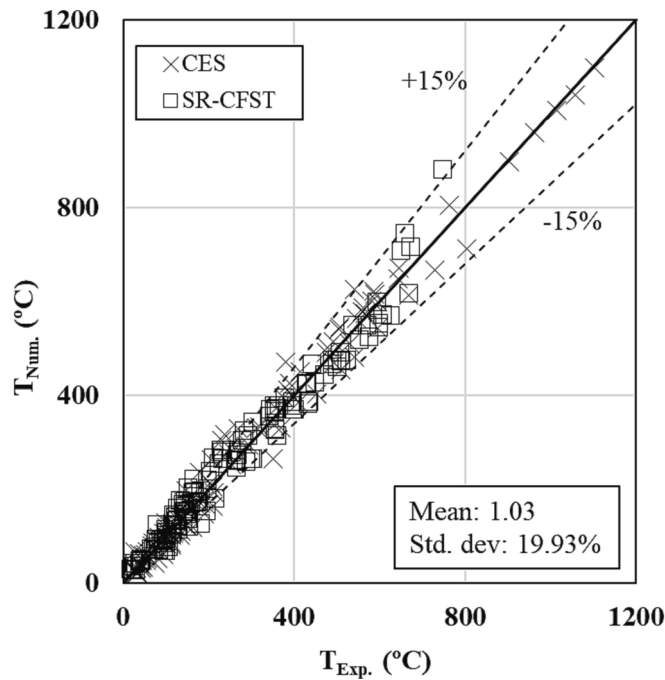

Fig. 13. Numerically predicted temperatures versus experimental temperatures at the available thermocouple locations for the different cases used for validation.

Table 2
Summary of the prediction errors in the validation of the thermal model ($\theta_{num}/\theta_{exp}$).

Section type	$\theta < 300$ °C		$\theta \geq 300$ °C		All range of θ	
	Mean	Std. dev.	Mean	Std. dev.	Mean	Std. dev.
All	1.06	0.24	0.99	0.08	1.03	0.20
SR-CFST	1.06	0.30	1.04	0.17	1.06	0.26
CES	1.03	0.26	1.01	0.08	1.02	0.21

4. Parametric studies on the thermo-mechanical response of SR-CFST columns

4.1. Composite sections used in the parametric study

A parametric study was carried out to analyse the influence of the different factors affecting the cross-sectional capacity of SR-CFST columns when subjected to fire. Table 3 shows the different column specimens studied.

The parameters varied were the outer dimension of the steel tube (D or B in the case of circular and square columns, respectively), the steel tube wall thickness (t) and the inner profile dimensions.

Two sets of cross-sections were analysed, the first set comprising 8 circular geometries and the second set including their 8 square counterparts. For comparison purposes, the outer tube dimensions were chosen so that all the circular/square pairs had approximately the same amount of steel area – from a catalogue range of commercially available sections, with differences below 2 % –. Two wall thicknesses were studied for each of the selected outer dimensions (thin and thick outer tube). It is worth noting that the hollow steel sections were designed to meet the criteria of non-slender sections, according to EN1993-1-1 [41], except for specimen CHS 508 × 8, which was not able to meet this criterion and was therefore classified as class 4. For each steel tube, different inner profiles were considered from the European vast flange beams catalogue. HEA and HEB sections were used, increasing their dimensions progressively. Two or three different inner profiles were studied for the wider hollow tubes, while for the narrower tubes, a single inner profile was chosen, given the spacing limitations within the section. In total, 120 case analyses were generated in these parametric studies: 60 column specimens with circular sections and other 60 with square sections.

Additionally, the influence of the concrete moisture content was studied in this investigation, covering three different values of moisture content: 4 %, 7 % and 10 %, so the total number of numerical simulations conducted amounts $120 \times 3 = 360$.

The nominal values of the steel yield strength and concrete compressive strength were assumed to be 355 MPa and 30 MPa, respectively (calcareous aggregates being considered for concrete). The steel and concrete grades were not varied in this analysis, since the main goal was to focus on the thermal response of the columns, rather than on the mechanical effects. The recommended values in EN 1994-1-2 [27] for steel and concrete thermal properties at elevated temperatures were used, except for the thermal conductivity of concrete, where the new proposal in prEN 1992-1-2:2021 [35] was adopted instead. Based on the previous sensitivity study results, a value of 200 W/m²K for the gap conductance at the steel–concrete interface was considered, while a perfect thermal contact was assumed at the inner profile-concrete interface.

4.2. Sectional integration for computing plastic resistance and stiffness

The SR-CFST sections had been previously discretised using a triangular mesh to carry out the thermal analysis (see Section 2.1). Therefore, the temperatures at the nodes of the FE mesh were known from the computed cross-sectional temperature field. As shown in Fig. 2, each triangular i-element of this mesh can be characterised by its position (z_i, y_i), area (A_i) and temperature (θ_i) – obtained by linear interpolation from nodal temperatures – and by the corresponding material properties for steel tube, concrete or inner profile. Thus, the cross-section plastic resistance and flexural stiffness for both major and minor axis bending at elevated temperatures can be integrated from cells using the following formulae:

$$N_{fi,pl,Rd} = \sum_{i=1}^{n} A_{a,i} \bullet k_{y_a,\theta_i} \bullet f_{y_a} + \sum_{i=1}^{n} A_{c,i} \bullet k_{c,\theta_i} \bullet f_c + \sum_{i=1}^{n} A_{p,i} \bullet k_{y_p,\theta_i} \bullet f_{y_p} \qquad (7)$$

Table 3
Summary of the analysis cases in the parametric studies.

(a) Circular Sections				(b) Square Sections		
D (mm)	*t* (mm)	Inner profile		*B* (mm)	*t* (mm)	Inner profile
193.7	4	HE100B		150	4	HE100B
	8				8	
219.1	4	HE120B		175	4	HE120B
	8				8	
273	5	HE140B		220	5	HE140B
	10				10	
323.9	6	HE140B–HE180B		260	6	HE140B – HE180B
	10				10	
355.6	6	HE100B–HE200B		300	6	HE100B–HE200B
	12.5				12.5	
406.4	7	HE120B–HE220B		325	7	HE120B–HE220B
	14.2				14.2	
457	8	HE100B–HE180B–HE280B		350	8	HE100–HE180B–HE280B
	10				10	
508	8	HE100B–HE200B–HE300B		400	8	HE100–HE200B–HE300B
	10				10	

Note: Same combinations repeated with inner HEA profiles.

$$EI_{z,fi} = \sum_{i=1}^{n} A_{a,i} \bullet y_i^2 \bullet k_{E_a,\theta_i} \bullet E_a + \sum_{i=1}^{n} A_{c,i} \bullet y_i^2 \bullet E_{c,sec,\theta_i} + \sum_{i=1}^{n} A_{p,i} \bullet y_i^2 \bullet k_{E_p,\theta_i} \bullet E_p \tag{8}$$

$$EI_{y,fi} = \sum_{i=1}^{n} A_{a,i} \bullet z_i^2 \bullet k_{E_a,\theta_i} \bullet E_a + \sum_{i=1}^{n} A_{c,i} \bullet z_i^2 \bullet E_{c,sec,\theta_i} + \sum_{i=1}^{n} A_{p,i} \bullet z_i^2 \bullet k_{E_p,\theta_i} \bullet E_p \tag{9}$$

where subscripts *a*, *c* and *p* correspond to the steel tube, concrete infill, and inner steel profile, respectively.

A numerical integration procedure was implemented through a Python subroutine and applied recurrently to all the analysed composite sections to compute their plastic resistance and flexural stiffness, as explained above.

The reduction factors for the mechanical properties of concrete and steel at their corresponding temperatures ($k_{y,\theta}$, $k_{c,\theta}$, $k_{E,\theta}$) were obtained from EN1994-1-2 [27]. It is worthy to note that the reduction factor for the concrete secant modulus (E_{c,sec,θ_i}) is not directly given in EN1994-1-2, nonetheless, it can be derived as follows:

$$E_{c,sec,\theta_i} = \frac{f_{c,\theta_i}}{\varepsilon_{cu,\theta_i}} = \frac{k_{c,\theta_i}}{\varepsilon_{cu,\theta_i}} \bullet f_c \tag{10}$$

In summary, once the nodal temperature was captured from the thermal FE analysis, the cross-sectional plastic resistance and stiffness were computed from eq. (7), (8) and (9) in order to carry out the comparisons in terms of mechanical capacity between the different column configurations in the parametric study.

4.3. Analysis of results of the parametric study

Fig. 14 to Fig. 17 present the evaluation of the parametric study results. Henceforth, the vertical axis represents the normalised cross-sectional plastic resistance of the columns at elevated temperature, referred to their room temperature value ($N_{fi,pl,Rd}/N_{pl,Rd}$).

The influence of the outer section shape (circular versus square), the outer hollow steel tube thickness (expressed in terms of the cross-sectional slenderness, D/t or B/t), the section factor (A_m/V) and the inner steel profile dimensions (measured through the "Inner Steel Contribution Ratio") is analysed in the following subsections.

Note that, in steel structures, the section factor (A_m/V) is defined as the fire exposed perimeter of the section divided by the total steel area. In this case, although the section is composite, the section factor can be defined as the fire exposed perimeter divided by the total area of the section (steel plus concrete), as already done for composite columns with partially encased steel sections in Annex G of EN 1994-1-2 [27] and

in the new method for CFST columns in Annex H of prEN 1994-1-2:2021 [42]. Henceforth, for a circular SR-CFST section it results $A_m/V = P_m/A = \pi D/(\pi D^2/4) = 4/D$, while for a square SR-CFST section it is equal to $A_m/V = P_m/A = 4B/B^2 = 4/B$.
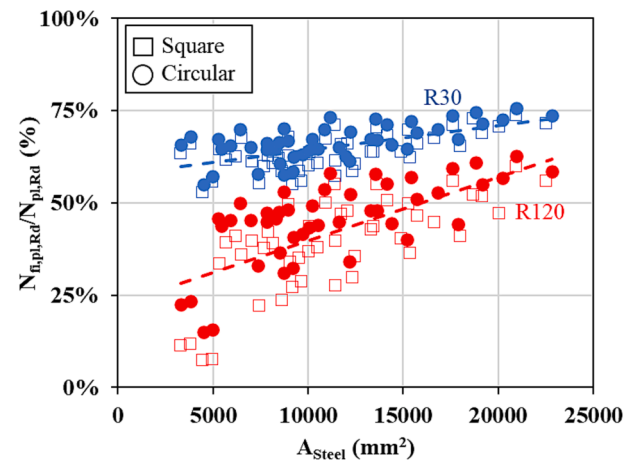

Fig. 14. Influence of the total steel area over the cross-sectional plastic resistance of the columns for both circular and square sections.
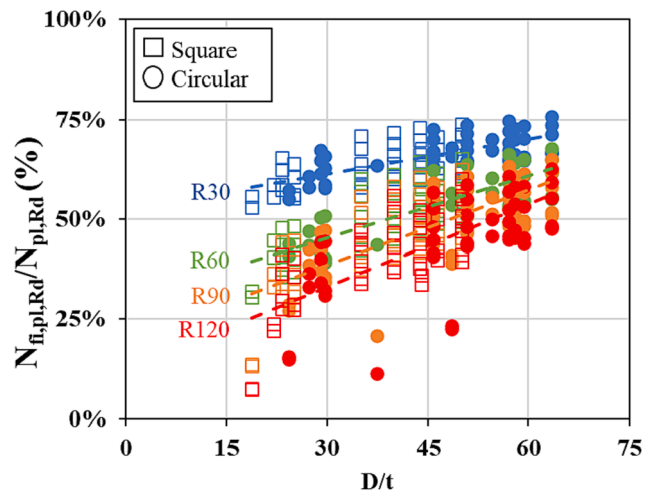

Fig. 15. Influence of the cross-sectional slenderness (*D/t*) over the plastic resistance of the columns, for both circular and square sections.
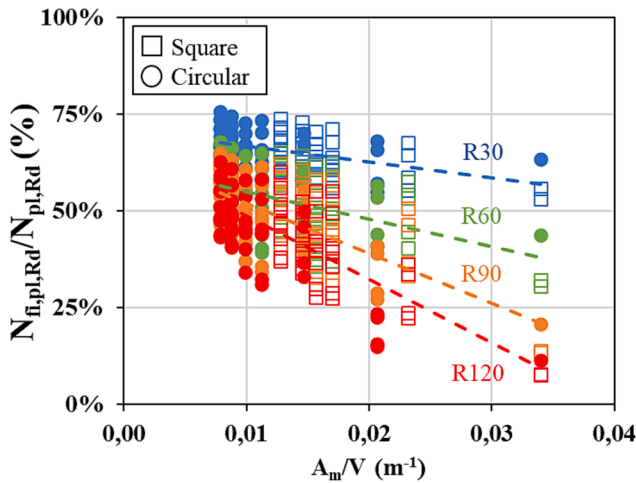
Fig. 16. Influence of the section factor (A_m/V) over the cross-sectional plastic resistance of the columns for both circular and square sections.
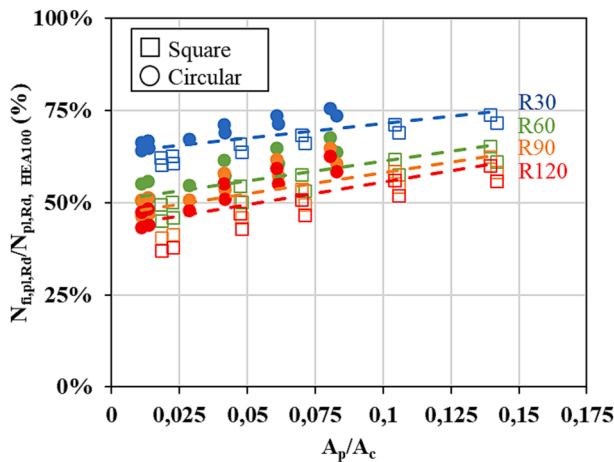

Fig. 17. Influence of the Inner Steel Contribution Ratio (ISCR) over the cross-sectional plastic resistance of the columns for sections CHS 508 mm × 8 mm and SHS 400 mm × 8 mm.

In turn, the "Inner Steel Contribution Ratio" (ISCR) has been defined by the authors as A_p/A_c (inner steel profile area divided by the concrete infill area) in order to quantify the amount of steel embedded in the concrete mass.

4.3.1. Influence of the outer section shape

Fig. 14 plots the results in terms of cross-sectional plastic resistance for the different series of columns studied, arranged by increasing the total steel area (steel tube + inner profile). It can be observed that the trend is positively linear, meaning that as the steel usage is increased, the mechanical capacity of the column rises. Additionally, this figure exhibits the differences between the circular and square cross-section shapes with the same steel usage, showing that the circular columns perform better under the effect of fire exposure. The reason for this behaviour is twofold: firstly, the lower section factor (A_m/V) of the circular columns provides them with a better thermal behaviour – i.e. slower temperature rise –, and secondly, the shortest distance between the inner face of the outer steel tube and the inner steel profile corner – i. e. concrete cover – is smaller in the square sections, which causes the heat to reach the steel H-section faster, which in turn explains its faster reduction in terms of load-bearing capacity.

The effect of the geometry becomes more pronounced as the fire exposure time is increased, resulting in a higher difference in axial capacity between the circular and square sections (note the difference for R120 as compared to R30).

4.3.2. Influence of the outer steel tube thickness

As shown in Fig. 15, the relationship between the cross-sectional slenderness (D/t) and the cross-sectional plastic resistance of the column is linearly positive for both square and circular sections. This effect can be explained by the fact that, as the D/t value is incremented, the area of steel at the outer surface is reduced (thinner hollow section), thus allowing for a more considerable amount of concrete infill and higher dimensions of the inner steel profile. Since it is directly exposed to fire, the outer steel tube is heavily affected by the temperature increase and rapidly loses its load-bearing capacity; therefore, the reduction of the amount of steel used in the outer tube and the increase in the dimensions of the inner profile – thermally protected by the concrete infill – enhances the cross-sectional capacity of the column.

4.3.3. Influence of the section factor

Fig. 16 shows the influence of the section factor (A_m/V) over the cross-sectional capacity of the columns. This parameter measures the amount of steel area exposed to the fire in relation to the heated volume and thus gives an idea of the influence of the outer sectional shape and dimensions over the thermal response of the columns. The section factor value affected the cross-sectional plastic resistance in a negative linear trend. As the A_m/V increases, the fire exposed perimeter of the cross-section also rises, causing the column to heat up faster, thus losing its mechanical properties at a faster pace than sections exposing a reduced perimeter to the fire. Note that for the same steel usage, the section factor (A_m/V) of the square columns is higher than that of their circular counterparts, thus explaining the faster temperature rise and mechanical deterioration of the square columns.

4.3.4. Influence of the dimensions of the inner profiles

The influence of the amount of steel used at the inner profiles was studied by varying the H-steel profile dimensions for a fixed size of the outer steel tube. Fig. 17 compares the different inner profiles analysed for the CHS 508 mm × 8 mm and the SHS 400 mm × 8 mm (inner profiles HE100A, HE200A, HE300A, HE100B, HE200B, HE300B). The results in terms of cross-sectional capacity are referred to the case with HE100A inner profile. They show the potential benefit of using an encased profile of higher dimensions, increasing the so-called "Inner Steel Contribution Ratio" (ISCR). Given these results, it becomes clear that the cross-sectional capacity of the columns, for any fire exposure time, is enhanced by the progressive increase in the ISCR for both circular and square sections.

Additionally, cross-sections with an HEB embedded profile have shown to have a higher mechanical capacity when compared to their HEA counterparts. This phenomenon is mainly due to the higher area of steel in HEB sections than HEA, which allows for a higher load-bearing capacity for the column.

4.3.5. Influence of the concrete moisture content

An analysis of the effect of the concrete moisture content over the cross-sectional plastic resistance of the columns was additionally conducted. Fig. 18 shows this effect for the case with outer CHS of diameter 194 mm and HEA100 inner profile, which was studied under three different values of moisture content: 4 %, 7 % and 10 %. As it was expected, the concrete moisture content has a favourable effect over the performance of the columns when exposed to fire, in the sense that as the moisture content increases, the temperature rise within the cross-section becomes slower and thus the mechanical capacity is increased. It can be observed that the increase in terms of cross-sectional plastic resistance capacity between the 4 % and 7 % models is remarkable, while for higher moisture contents this effect is less pronounced.
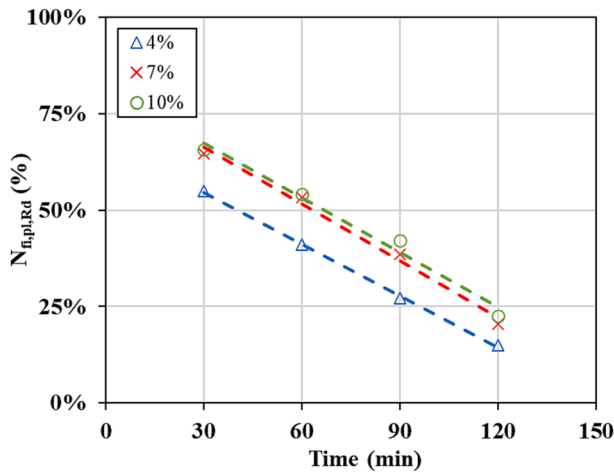
Fig. 18. Influence of the concrete moisture content over the cross-sectional plastic resistance of the columns for both circular and square sections.

4.3.6. Summary of the analysis results

Through this analysis, it was found that the development of temperatures across the section is highly affected by the section factor value (A_m/V), with a faster increase of temperatures for those columns with higher section factors (i.e. small diameters), which expose a relatively high surface to the fire for the same volume and thus heat up faster. This effect ultimately affects the cross-sectional plastic resistance of the columns, leading to higher capacities for the columns with lower section factors. The variation of the inner steel profile dimensions also influenced positively the thermal behaviour of the column as the ISCR parameter was increased (i.e. higher dimensions of the inner steel profile). It was also observed that a change in the steel tube wall thickness influenced the thermal response of the columns, in the sense that a lower steel tube wall thickness benefits the mechanical capacity of the composite section, provided that the amount of steel removed from the outer tube is introduced at the inner steel profile.

Finally, regarding the influence of the concrete moisture content, it was observed that a higher value of this parameter was beneficial for the thermal response of the section. Therefore, the most conservative concrete moisture content value of 4 % will be assumed in the subsequent design proposal, as recommended in Clause 3.3.2(7) of EN1994-1-2 [27].

All these findings will be used in the following section for developing a simplified proposal for predicting the temperature field in SR-CFST columns.

5. Development of a simplified temperature distribution proposal for Steel-reinforced CFST sections

In evaluating a steel–concrete composite section under fire based on the provisions of EN 1994-1-2 [27], it is required to compute the cross-sectional temperature field after a given duration of fire exposure. However, the code does not provide any simplified process to obtain the temperature field of the cross-section quickly. This chapter presents a simple method to evaluate the temperature field within an SR-CFST column, which may help practitioners in this task.

It is intended to obtain a uniform equivalent temperature for the whole concrete core ($\theta_{c,eq}$), the web and the flanges of the embedded steel profile ($\theta_{w,eq}$ and $\theta_{f,eq}$) and the outer steel tube ($\theta_{a,eq}$) to get the exact fire resistance of the column which would be obtained by using the actual non-uniform temperature distribution. The benefit of this approach is that the designer can evaluate the fire resistance of the cross-section by using a single strength and stiffness value for each component of the composite cross-section corresponding to its temperature. The authors previously used this approach for developing a temperature

distribution proposal for CFST columns [26] which has been recently included in the draft version of the new Eurocode 4 Part 1.2 (prEN 1994-1-2:2021) [42]. The calculation procedure is described hereafter.

5.1. Previous simplified methods for predicting the temperature field of composite sections

Annex G of EN 1994-1-2 [27] presents a simplified temperature model to calculate the fire resistance of composite columns with partially encased steel sections uniformly exposed to fire. This method shows four different temperatures corresponding to the concrete area, the reinforcing bars, steel profile web and flanges. The concrete core and steel profile flanges temperature correlate with the standard fire resistance time (R) and the column section factor (A_m/V). For the reinforcing bars, the method provides the reduction factors for the steel yield strength and modulus of elasticity directly, depending on the standard fire resistance time (R) and the geometrical average of the axis distance of the reinforcement to the outer concrete surface (u_s).

The method used on the web of the embedded steel profile is significantly different from that used at the flanges. EN 1994-1-2 Annex G [27] states that, to consider the effect of temperature on the material properties, a part of the web may be neglected, thus reducing the material properties of the flange itself. Therefore, the height reduction of the profile web is given as a function of the standard fire resistance time; thus, the design plastic resistance and flexural stiffness can be worked out after removing this part of the web.

This approach was tentatively applied to the inner profiles and concrete infill of the SR-CFST sections studied in this paper by introducing some adaptations. However, as the method is developed explicitly for partially encased sections (i.e. without outer steel tube and with the inner steel profile flanges directly exposed to the fire), the predicted temperature distributions were far from realistic, as shown in Fig. 19.

Regarding the fire design of CFST columns, the authors of this paper previously proposed an innovative design method [26] which was approved by the Technical Committee CEN/TC250/SC4 [43] to be included in the new version of Eurocode 4 Part 1.2 (prEN 1994-1-2:2021) [41] in replacement of the current Annex H. This method presents three different equations to obtain the equivalent temperatures of
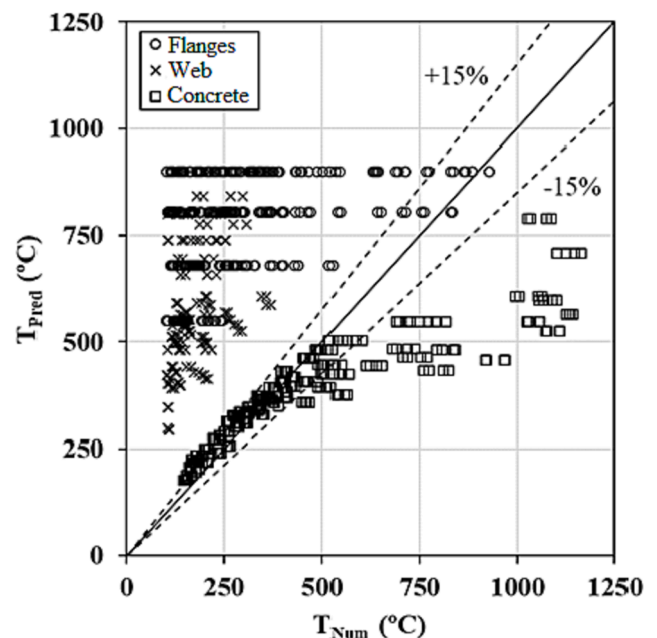

Fig. 19. Comparison between predicted and numerical temperatures at the different parts of the composite section using the equations from Annex G of EN 1994-1-2 [24].

the main components of the cross-section: the concrete core, the outer steel tube and the reinforcement bars. According to the proposed equations, the concrete infill and the outer steel tube equivalent temperatures were highly associated with the standard fire exposure time (R) and the section factor (A_m/V).

On the other hand, a different approach was adopted to obtain the equivalent temperature of the reinforcing bars, based on previous works on the development of temperature fields in concrete structures subjected to fire by Wickström [44]. The reinforcing bars' temperature was strongly correlated to the parameter R/u_s^2, being u_s the concrete cover, measured from the axis distance of the reinforcing bars to the exposed surface of the concrete.

Some parts of the existing temperature proposal for CFST columns developed by the authors [26] will be adapted here to SR-CFST sections, such as the equivalent temperature equation for the outer steel tube or the shape of the function for the concrete infill, as the temperature field in these parts of the section is similar.

5.2. Simplified cross-sectional temperature field proposal for SR-CFST sections

A multivariant regression analysis was performed, based on the results of the previously presented study on the influence of specific parameters.

This section aims to characterise the SR-CFST cross-section temperature field in a simple but practical way by obtaining an equivalent temperature for each part of the composite cross-section: the outer steel tube ($\theta_{a,eq}$), the concrete infill ($\theta_{c,eq}$), the inner steel profile web ($\theta_{w,eq}$) and flanges ($\theta_{f,eq}$). Fig. 20 shows the definition of the equivalent temperatures associated with their corresponding parts.

5.2.1. Calculation of the equivalent temperature for the outer steel tube

For the outer steel tube, the equivalent temperature at each standard fire time was directly obtained from the numerical analyses by calculating the average value of the temperatures at both inner and outer surfaces. This temperature was almost uniform through the steel tube wall thickness for each standard fire period.

The equation previously proposed by the authors in the design method for CFST columns [26] to obtain the equivalent temperature of the outer steel tube was tested in this study, producing an average error of 1.005 for the circular specimens with a 1.28 % standard deviation and an average error of 1.021 with 1.26 % standard deviation for the square ones, therefore considering it accurate enough to be applied to SR-CFST columns. The specified formula is given hereafter:

$$\theta_{a,eq} = -824.667 - 5.579R + 0.007R^2 - 0.009R \bullet A_m/V + 645.076$$
$$\bullet R^{0.269} \bullet (A_m/V)^{0.017} \tag{11}$$

Alternatively, a selection chart is given in Table 5 to obtain directly the outer steel tube temperature.

Fig. 21 compares the calculated and numerically predicted temperatures at the outer steel tube. Since the temperatures obtained with the equation are highly correlated with those extracted from the parametric study, the formula is considered valid for the column typologies analysed in this study.

5.2.2. Calculation of the equivalent temperature for the concrete infill

The equivalent temperature representing the concrete infill can be derived through two different approaches, by using either the plastic resistance or the flexural stiffness of the whole concrete part:

a) Plastic resistance approach.

The plastic resistance to axial compression of the concrete infill in the fire situation is equal to:

$$N_{fi,pl,Rd,c} = \sum_{i=1}^{n}(A_{c,i} \bullet f_{c,\theta_i}) = \sum_{i=1}^{n}(A_{c,i} \bullet k_{c,\theta_i} \bullet f_c) = f_c \bullet \sum_{i=1}^{n}(A_{c,i} \bullet k_{c,\theta_i}) \tag{12}$$

A single equivalent temperature is needed, which produces the same plastic resistance through its corresponding reduction factor when applied to the whole concrete infill:

$$N_{fi,pl,Rd,c} = f_c \bullet \sum_{i=1}^{n}(A_{c,i} \bullet k_{c,\theta_i}) = k_{c,\theta}(\theta_{c,eq1}) \bullet f_c \bullet A_c \rightarrow k_{c,\theta}(\theta_{c,eq1})$$
$$= \frac{\sum_{i=1}^{n}(A_{c,i} \bullet k_{c,\theta_i})}{A_c} \tag{13}$$

Once this reduction coefficient is calculated, the equivalent temperature $\theta_{c,eq1}$ representing the whole concrete part can be found in Table 3.3 in EN 1994-1-2 [27] using linear interpolation.

b) Flexural stiffness approach (major axis bending).

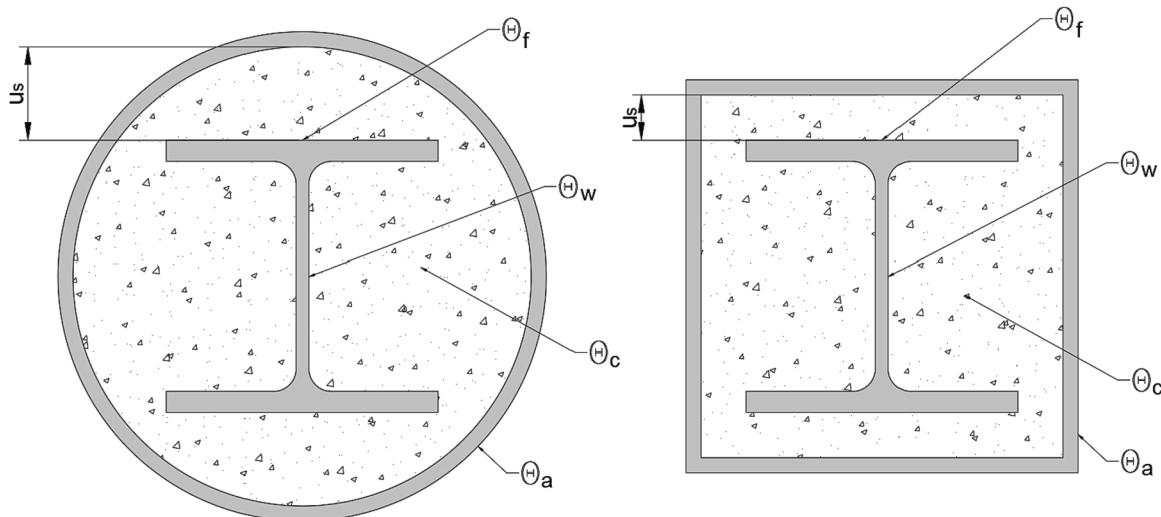The flexural stiffness of the concrete infill in the fire situation for major axis bending is equal to:

Fig. 20. Equivalent temperatures of the different parts of the composite section and definition of the parameter us in circular and square SR-CFST columns.
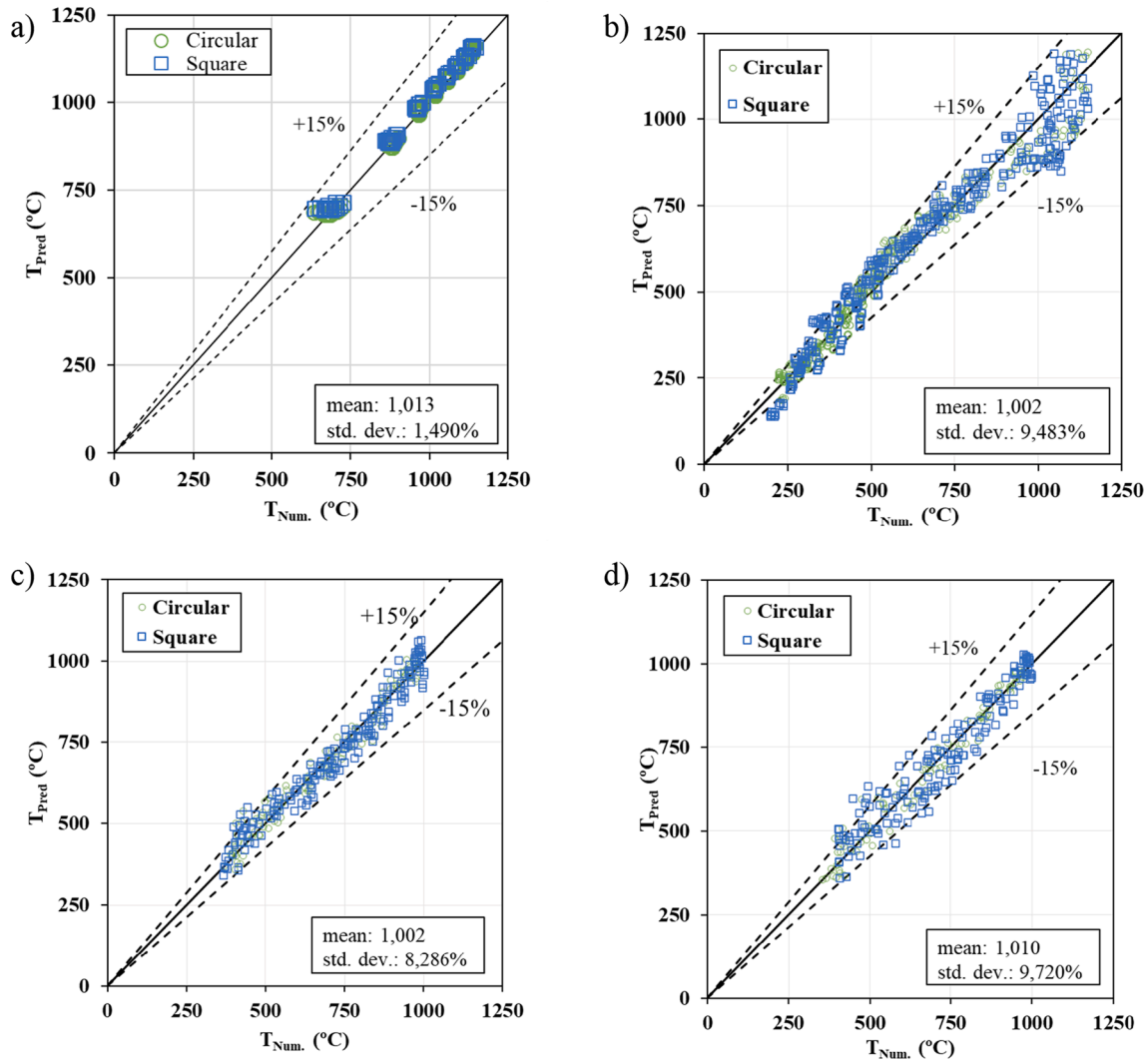
Fig. 21. Comparison between predicted equivalent temperature and numerical temperature: (a) outer steel tube, (b) concrete infill, (c) inner steel profile flanges and (d) inner steel profile web.

$$EI_{z,fi,c} = \sum_{i=1}^{n}\left(I_{z,c,i} \bullet E_{c,sec,\theta_i}\right) = \sum_{i=1}^{n}\left(I_{z,c,i} \bullet \frac{f_{c,\theta,i}}{\varepsilon_{cu,\theta,i}}\right) = \frac{f_c}{\varepsilon_{cu}} \bullet \sum_{i=1}^{n}\left(I_{z,c,i} \bullet \frac{k_{c,\theta,i}}{\frac{\varepsilon_{cu,\theta,i}}{\varepsilon_{cu}}}\right)$$

$$= E_{c,sec} \bullet \sum_{i=1}^{n}\left(I_{z,c,i} \bullet k_{Ec,\theta,i}\right)$$

(14)

with $k_{Ec,\theta,i} = k_{c,\theta,i} \bullet \varepsilon_{cu}/\varepsilon_{cu,\theta,i}$.

It is required to obtain an equivalent temperature that produces the same flexural stiffness through its corresponding reduction factor when applied to the whole concrete part:

$$EI_{z,fi,c} = E_{c,sec} \bullet \sum_{i=1}^{n}\left(I_{z,c,i} \bullet k_{Ec,\theta,i}\right) = k_{Ec,\theta}\left(\theta_{c,eq2}\right) \bullet E_{c,sec} \bullet I_{z,c} \rightarrow k_{Ec,\theta}\left(\theta_{c,eq2}\right)$$

$$= \frac{\sum_{i=1}^{n}\left(I_{z,c,i} \bullet k_{Ec,\theta,i}\right)}{I_{z,c}}$$

(15)

In this type of geometry, the column section is not symmetric. As a result, the flexural stiffness of the concrete must be calculated for both axes using the same method for the minor axis bending. The equivalent temperatures for the concrete infill resulting from applying this procedure to both axes are $\theta_{c,eq2}$ and $\theta_{c,eq3}$, which can be obtained through Table 3.3 in EN 1994-1-2 [27] by using linear interpolation and considering $k_{Ec,\theta} = k_{c,\theta} \bullet \varepsilon_{cu}/\varepsilon_{cu,\theta}$.

Conservatively, the equivalent temperature of the concrete infill will be defined as the maximum of the temperatures obtained through the three approaches described above:

$$\theta_{c,eq} = max\{\theta_{c,eq1}, \theta_{c,eq2}, \theta_{,eq3}\}$$

(16)

A single equation for the equivalent temperature of concrete valid for any fire resistance period was developed by using a multiple nonlinear regression analysis, which includes the effect of A_m/V, A_{sp}/A_c, and R:

$$\theta_{c,eq} = a_1 + b_1R + b_2R^2 + c_1(A_m/V) + c_2\left(\frac{A_m}{V}\right)^2 + d_1R(A_m/V) + e_1R^{f1}\left(\frac{A_m}{V}\right)^{f2}$$

$$+ g_1R(A_{sp}/A_c)$$

$$\leq 1200^\circ C$$

(17)

where coefficients a_1 to g_1 depend on the shape of the section (circular or square) and are given in Table 4. A temperature plateau was set at 1200 °C due to the loss of structural capacity of concrete above this value. This equation can be used as an alternative to the selection chart .

A comparison between calculated and numerically predicted temperatures at the concrete infill can be observed in Fig. 21(a).

Alternatively, a selection chart is given in Table 6 for circular sections and Table 7 for square sections to facilitate designers in obtaining the equivalent temperature of the concrete infill for a particular fire

Table 4

Coefficients for the equivalent temperature of the concrete infill $\theta_{c,eq}$ (°C), flanges $\theta_{f,eq}$ (°C) and web $\theta_{w,eq}$ (°C) of the inner steel profile.

		a_1	b_1	b_2	c_1	c_2	d_1	e_1	f_1	f_2	g_1	g_2
CONCRETE	CIRC	1120,11	−10,14	7,80E−03	−145,94	4,05	1,30	−1,83E−05	1,91	2,84	5,17	–
	SQUA	865,60	−23,88	2,91E−02	−93,38	1,55	5,88	−1,54	1,09	1,20	4,70	–
FLANGES	CIRC	−1174,15	14,08	−2,03E−02	59,59	2,12E−02	−5,84E−02	9,53E−05	1,83	1,86	9,27	–
	SQUA	794,25	−7,19	9,83E−03	−81,30	1,26	7,59	−4,51	1,05	1,06	−9,64	–
WEB	CIRC	3267,34	3,24	0,01	184,79	−5,30	3,59	−1,29	1,18	1,01	10891,6	−55465,4
	SQUA	−941,09	−5,32	6,62E−03	−22,25	0,36	3,41	−1,17	1,10	1,12	6939,91	−19679,4

Table 5

Selection chart for the equivalent temperature of the outer steel tube $\theta_{a,eq}$ (°C) (extracted from [15]).

		R30	R60	R90	R120	R180	R240
A_m/V (m^{-1})	5	669	858	951	1005	1070	1125
	10	687	879	973	1028	1094	1149
	15	697	890	984	1039	1105	1158
	20	704	897	992	1046	1110	1162
	25	709	903	996	1050	1112	1162
	30	713	906	999	1052	1113	1162
	35	716	909	1001	1053	1113	1162
	40	719	911	1002	1054	1113	1162
	45	721	912	1003	1054	1113	1162

period directly from the value of the section factor of the column. For intermediate values of the section factor and the inner steel contribution ratio, linear interpolation can be used.

5.2.3. Calculation of the equivalent temperature for the inner steel profile

Concerning the temperature of the inner steel profile, it has been observed that the temperatures obtained at the flanges differ significantly from the ones obtained on the web. Thus, two equivalent temperatures will be proposed in this study: one for the web and another one for the flanges.

The procedure to obtain the equivalent temperature at the flanges and the web of the steel profile was like that applied for deriving the equivalent temperature of the concrete infill. Both parts (flanges and web) were calculated separately by isolating the cells corresponding to each zone and processing them individually.

a) Plastic resistance approach.

The plastic resistance to axial compression of the inner steel profile parts under elevated temperature conditions can be obtained by using the following formulae:

$$N_{fi,pl,Rd,f} = \sum_{i=1}^{n}(A_{f,i} \bullet f_{s,\theta_i}) = \sum_{i=1}^{n}(A_{f,i} \bullet k_{s,\theta_i} \bullet f_s) = f_s \bullet \sum_{i=1}^{n}(A_{f,i} \bullet k_{s,\theta_i}) \qquad (18)$$

$$N_{fi,pl,Rd,w} = \sum_{i=1}^{n}(A_{w,i} \bullet f_{s,\theta_i}) = \sum_{i=1}^{n}(A_{w,i} \bullet k_{s,\theta_i} \bullet f_s) = f_s \bullet \sum_{i=1}^{n}(A_{w,i} \bullet k_{s,\theta_i}) \qquad (19)$$

By isolating the reduction factor in this equation, it can be derived by performing a sectional integration process:

$$N_{fi,pl,Rd,f} = f_s \bullet \sum_{i=1}^{n}(A_{f,i} \bullet k_{s,\theta_i}) = k_{s,\theta}(\theta_{f,eq1}) \bullet f_s \bullet A_f \rightarrow k_{s,\theta}(\theta_{f,eq1})$$
$$= \frac{\sum_{i=1}^{n}(A_{f,i} \bullet k_{s,\theta_i})}{A_f} \qquad (20)$$

$$N_{fi,pl,Rd,w} = f_s \bullet \sum_{i=1}^{n}(A_{w,i} \bullet k_{s,\theta_i}) = k_{s,\theta}(\theta_{w,eq1}) \bullet f_s \bullet A_w \rightarrow k_{s,\theta}(\theta_{w,eq1})$$
$$= \frac{\sum_{i=1}^{n}(A_{w,i} \bullet k_{s,\theta_i})}{A_w} \qquad (21)$$

The equivalent temperatures of the steel profile flanges and web, $\theta_{f,eq1}$ and $\theta_{w,eq1}$, respectively, can be obtained using linear interpolation in

Table 6

Selection chart for the equivalent temperature of the concrete infill $\theta_{c,eq}$ (°C) for circular sections.

A_p/A_c		0,01						0,05						0,1					
		R30	R60	R90	R120	R180	R240	R30	R60	R90	R120	R180	R240	R30	R60	R90	R120	R180	R240
A_m/V (m^{-1})	10	<200	237	323	410	589	775	<200	249	341	435	626	825	<200	265	365	466	672	887
	15	<200	336	538	713	988	1165	<200	348	557	738	1025	>1200	<200	364	580	769	1072	>1200
	20	245	580	832	1005	1125	>1200	252	592	850	1030	1162	>1200	259	608	874	1061	>1200	

Table 7

Selection chart for the equivalent temperature of the concrete infill $\theta_{c,eq}$ (°C) for square sections.

A_p/A_c		0,02						0,1						0,2					
		R30	R60	R90	R120	R180	R240	R30	R60	R90	R120	R180	R240	R30	R60	R90	R120	R180	R240
A_m/V (m^{-1})	10		<200	<200	<200	<200	360		<200	<200	<200	239	450		<200	<200	213	324	563
	15	<200	275	381	477	690	979	<200	297	415	522	758	1069	<200	325	457	578	843	1182
	20	<200	392	572	715	966	>1200	<200	415	606	760	1034	>1200	<200	443	648	816	1119	>1200
	25	<200	512	722	868	1066	>1200	<200	534	755	913	1134	>1200	<200	562	798	969	>1200	
	30	278	645	850	962	>1200		289	667	884	1008	>1200		303	696	926	1064	>1200	

Table 3.2 in EN 1994-1-2 [27].

b) Flexural stiffness approach.

The flexural stiffness of the inner steel profile parts under fire conditions for major axis bending can be calculated through the following equation:

$$EI_{z,fi,f} = \sum_{i=1}^{n}(I_{z,f,i} \bullet E_{a,\theta}) = \sum_{i=1}^{n}(I_{z,f,i} \bullet k_{E,\theta}(\theta_{f,eq2}) \bullet E_a)$$
$$= E_a \bullet \sum_{i=1}^{n}(I_{z,f,i} \bullet k_{E,\theta}(\theta_{f,eq2})) \tag{22}$$

$$EI_{z,fi,w} = \sum_{i=1}^{n}(I_{z,w,i} \bullet E_{a,\theta}) = \sum_{i=1}^{n}(I_{z,w,i} \bullet k_{E,\theta}(\theta_{w,eq2}) \bullet E_a)$$
$$= E_a \bullet \sum_{i=1}^{n}(I_{z,w,i} \bullet k_{E,\theta}(\theta_{w,eq2})) \tag{23}$$

Subsequently, the flexural stiffness reduction coefficient is obtained:

$$EI_{z,fi,f} = E_a \bullet \sum_{i=1}^{n}(I_{z,f,i} \bullet k_{E,\theta}(\theta_{f,eq2})) = k_{E,\theta}(\theta_{f,eq2}) \bullet E_a \bullet I_{z,f} \rightarrow k_{E,\theta}(\theta_{f,eq2})$$
$$= \frac{\sum_{i=1}^{n}(I_{z,f,i} \bullet k_{E,\theta,i})}{I_{z,f}} \tag{24}$$

$$EI_{z,fi,w} = E_a \bullet \sum_{i=1}^{n}(I_{z,w,i} \bullet k_{E,\theta}(\theta_{w,eq2})) = k_{E,\theta}(\theta_{w,eq2}) \bullet E_a \bullet I_{z,w} \rightarrow k_{E,\theta}(\theta_{w,eq2})$$
$$= \frac{\sum_{i=1}^{n}(I_{z,w,i} \bullet k_{E,\theta,i})}{I_{z,w}} \tag{25}$$

This procedure is replicated for minor axis bending, given the asymmetric cross-section distribution, thus obtaining another two sets of equivalent temperatures corresponding to each part of the steel profile: $\theta_{f,eq3}$, and $\theta_{w,eq3}$. Equivalent temperatures $\theta_{f,eq2}$, $\theta_{w,eq2}$, $\theta_{f,eq3}$ and $\theta_{w,eq3}$ can be extracted from Table 3.2 in EN 1994-1-2 [27] by applying linear interpolation.

The representative equivalent temperature for the flange and the web is taken as the maximum of the three temperatures obtained from the described procedure:

$$\theta_{f,eq} = max\{\theta_{f,eq1}, \theta_{f,eq2}, \theta_{f,eq3}\} \tag{26}$$

$$\theta_{w,eq} = max\{\theta_{w,eq1}, \theta_{w,eq2}, \theta_{w,eq3}\} \tag{27}$$

Equivalent temperature for the flanges of the inner steel profile

An additional parameter was introduced to quantify the concrete cover around the flanges of the inner steel profile, which was found to influence their temperature strongly. This parameter, defined as u_s, measures the distance between the flanges of the embedded steel profile and the inner surface of the hollow steel tube, as defined in Fig. 220.

The equivalent temperature of the inner steel profile flanges is obtained by using multiple nonlinear regression analyses, including the effect of A_m/V, u_s, and R:

$$\theta_{f,eq} = a_1 + b_1R + b_2R^2 + c_1(A_m/V) + c_2(A_m/V)^2 + d_1R(A_m/V) + e_1R^{f1}(A_m/V)^{f2} + g_1u_s \tag{28}$$

where coefficients a_1 to g_1 depend on the section shape (circular or square), see Table 4.

Fig. 21(b) shows the comparison between the calculated and numerically predicted temperatures at the flanges of the inner profile.

Additionally, two equivalent temperature tables are presented in Table 8 and Table 9 (for circular and square sections, respectively), which can be an alternative to applying the previously presented equations. For the section factor (A_m/V) and concrete cover (u_s), linear interpolation can be used on intermediate values.

Equivalent temperature for the web of the inner steel profile

Besides the standard fire time (R) and the section factor (A_m/V), the ISCR parameter was relevant when analysing the web temperature. Thus, a similar formula was obtained for the equivalent temperature of the steel profile web, which includes the effect of A_m/V, A_{sp}/A_c, and R:

$$\theta_{w,eq} = a_1 + b_1R + b_2R^2 + c_1(A_m/V) + c_2(A_m/V)^2 + d_1R(A_m/V) + e_1R^{f1}(A_m/V)^{f2} + g_1(A_{sp}/A_c) + g_2(A_{sp}/A_c)^2 \tag{29}$$

where coefficients a_1 to g_2 depend on the cross-section shape (circular or square), see Table 4.

A comparison between the calculated and numerically predicted temperatures at the web of the steel profile can be observed in Fig. 21(c).

Two equivalent temperature tables are also given (Table 10 for circular and Table 11 for square sections), which can serve as an alternative design method. Linear interpolation can be used for intermediate values of the section factor and the ISCR.

5.3. Applicability limits of the proposed method

The previously given equivalent temperature equations should only be applied for SR-CFST columns which meet the following requirements:

- For circular SR-CFST columns:

$8m^{-1} \leq A_m/V \leq 20m^{-1}$

$24 \leq D/t \leq 64$

$0,011 \leq A_p/A_c \leq 0,108$

- For square SR-CFST columns:

$13m^{-1} \leq A_m/V \leq 34m^{-1}$

Table 8
Selection chart for the equivalent temperature of the flanges of the inner steel profile $\theta_{f,eq}$ (°C) for circular sections.

A_m/V (m⁻¹)	10						20					
u_s (mm)	R30	R60	R90	R120	R180	R240	R30	R60	R90	R120	R180	R240
15			<400	569	966	>1200	<400	544	791	986	>1200	>1200
30			<400	430	827	1063	<400	405	652	847	1083	1117
45				<400	688	924		<400	513	708	944	978
60		<400		<400	549	785			<400	569	805	839
75				<400	410	646	<400		<400	430	666	700
90					<400	507				<400	527	561

Table 9
Selection chart for the equivalent temperature of the flanges of the inner steel profile $\theta_{f,eq}$ (°C) for square sections.

A_m/V (m⁻¹)	15						30					
u_s (mm)	R30	R60	R90	R120	R180	R240	R30	R60	R90	R120	R180	R240
15		<400	515	655	883	1079	<400	497	748	913	1077	1096
30			<400	510	738	934		<400	604	769	932	952
45				<400	594	789		<400	459	624	788	807
60		<400		<400	449	645			<400	480	643	663
75					<400	500	<400			<400	499	518
90						<400				<400	<400	<400

Table 10
Selection chart for the equivalent temperature of the inner steel profile web $\theta_{w,eq}$ (°C) for circular sections.

A_p/A_c	0,01						0,05						0,1					
A_m/V (m⁻¹)	R30	R60	R90	R120	R180	R240	R30	R60	R90	R120	R180	R240	R30	R60	R90	R120	R180	R240
10						<400					<400	<400		<400			<400	464
15		<400			<400	432		<400		<400	552	734			<400	<400	681	863
20				<400	492	551			<400	552	795	853			<400	458	681	923	982

Table 11
Selection chart for the equivalent temperature of the inner steel profile web $\theta_{w,eq}$ (°C) for square sections.

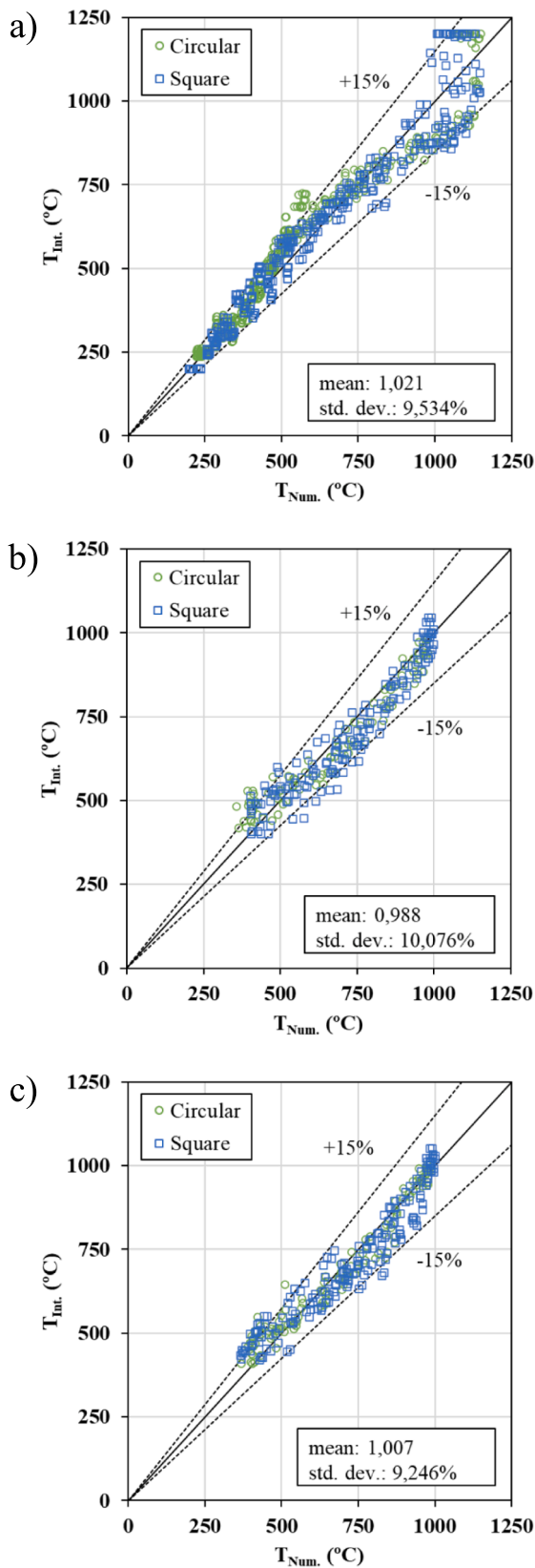| A_p/A_c	0,02						0,1						0,2					
A_m/V (m⁻¹)	R30	R60	R90	R120	R180	R240	R30	R60	R90	R120	R180	R240	R30	R60	R90	R120	R180	R240
10											<400	<400					<400	<400
15		<400				<400		<400		<400	418	606		<400		<400	522	710
20				<400	437				<400	634	803			<400	493	738	907
25			<400	413	530			<400	551	779	896		<400	479	654	882	1000
30			<400	502	541	<400	511	683	868	907	<400	614	787	972	1011

Fig. 22. Comparison between predicted and linearly interpolated temperature: (a) concrete infill, (b) inner steel profile flanges and (c) inner steel profile web.

$19 \le B/t \le 50$

$0,018 \le A_p/A_c \le 0,204$

- The method can be used for standard fire exposure times ranging between 30 and 240 min.

5.4. Verification of the proposed design method

A final verification step was conducted to check the accuracy of the presented method in predicting the temperature field of SR-CFST. Several analysis cases selected from the parametric study database were used as check points for the model, and the equivalent temperatures for the different parts of the composite section were obtained by linearly interpolating in the presented design tables. Fig. 22 shows the comparison between the interpolated temperatures and the numerically computed ones at certain locations of the cross-section. The mean and standard deviation values of the prediction errors obtained for the concrete core, inner steel profile flanges and web are also given in the figure.

As can be seen, the method provides a good prediction accuracy within its applicability boundaries. It covers and extensive range of application, considering long fire exposure times (up to 240 min) and a wide range of cross-sectional dimensions.

6. Summary and conclusions

This paper presented a numerical investigation of the thermal behaviour of SR-CFST columns exposed to fire. The authors developed a sectional FE model using the nonlinear analysis software package ABAQUS and validated against several SR-CFST and CES specimens from experimental campaigns available in the literature.

Once validated, the numerical model was used to conduct a parametric study comprising 120 analysis cases. An evaluation of the influence of several parameters on the cross-sectional plastic resistance of the SR-CFST columns was performed. These parameters were the section shape (circular or square), the outer steel tube thickness, the section factor, and the Inner Steel Contribution Ratio (ISCR). A numerical integration procedure was developed by the authors through a Python subroutine and recurrently applied to compute the plastic resistance and flexural stiffness of all the analysed composite sections as a summation of the cells of the FE mesh, taking into account the degraded properties of steel and concrete at elevated temperature, which were assigned to the different cells from the previously computed cross-sectional temperature field at each standard fire period.

The parametric analyses found that the circular columns performed better under the effect of fire exposure, and this effect was more pronounced as the fire exposure time increased. For the same steel usage, the section factor of the square columns was higher than that of their circular counterparts, thus explaining their faster temperature rise and mechanical deterioration. It was also found that the reduction of the outer steel tube thickness and the increase in the dimensions of the inner steel profile incremented the mechanical capacity of the columns at elevated temperatures. Moreover, the cross-sectional capacity of the columns was enhanced by the progressive increase in the ISCR for both circular and square sections.

An innovative design method for determining the cross-sectional temperature field of unprotected SR-CFST columns under iSO-834 standard fire conditions was also presented in this paper. The developed equivalent temperature equations cover an existing limitation in EN 1994-1-2 regarding the lack of a temperature distribution proposal for specific steel–concrete composite sections, such as SR-CFST. The

proposed method provides designers with a user-friendly tool to quickly calculate the cross-sectional temperature field of these composite sections for the subsequent application of the reduction coefficients of the steel and concrete parts degraded by their temperatures. A single equivalent temperature representing the outer steel tube, concrete infill, inner steel profile web and flanges can be obtained through the proposed equations and tables. This way, the sectional capacity of a SR-CFST column exposed to fire can be easily computed as at room temperature (i.e. by adding the contribution of each component of the section) but simply reducing the capacity of each part according to its assigned equivalent temperature.

This proposal can be very helpful in the fire design process of steel–concrete composite structures, providing an accessible and simple tool for practitioners, while it has the potential to be further expanded for considering other cross-section types and geometries.

CRediT authorship contribution statement

David Medall: Conceptualization, Methodology, Validation, Formal analysis, Investigation, Writing – original draft. **Ana Espinós:** Conceptualization, Methodology, Investigation, Writing – review & editing, Funding acquisition, Project administration. **Vicente Albero:** Conceptualization, Methodology, Investigation, Writing – review & editing. **Manuel L. Romero** Conceptualization, Supervision, Funding acquisition, Project administration, Investigation.

Declaration of Competing Interest

The authors declare that they have no known competing financial interests or personal relationships that could have appeared to influence the work reported in this paper.

Data availability

Data will be made available on request.

Acknowledgements

References

[1] Espinos A, Romero ML, Serra E, Hospitaler A. Circular and square slender concrete-filled tubular columns under large eccentricities and fire. J Constr Steel Res 2015;110:90–100. https://doi.org/10.1016/j.jcsr.2015.03.011.
[2] Romero ML, Espinós A, Lapuebla-Ferri A, Albero V, Hospitaler A. Recent developments and fire design provisions for CFST columns and slim-floor beams. J Constr Steel Res 2020;172:106159. https://doi.org/10.1016/j.jcsr.2020.106159.
[3] Zhou G, Luo C, Chen C, Dong X, Chen X, Liu X. The structural design of the Haiyi Hotel in Jiangmen. Guangdong Architect Civ Eng 2014:3–7.
[4] Romero ML, Espinós A, Renaud C, Bihina G, Schaumann P, Kleiboemer I et al. Fire resistance of innovative and slender concrete filled tubular composite columns (FRISCC). Final Report. Catalogue Number KI-NA-28082-EN-N. Brussels: RFCS Publications; 2016.
[5] Ferdous W, Bai Y, Almutairi AD, Satasivam S, Jeske J. Modular assembly of water-retaining walls using GFRP hollow profiles: components and connection performance. Compos Struct 2018;194. doi: 10.1016/j.compstruct.2018.03.074.
[6] Ferdous W, Almutairi AD, Huang Y, Bai Y. Short-term flexural behaviour of concrete filled pultruded GFRP cellular and tubular sections with pin-eye connections for modular retaining wall construction. Compos Struct 2018;206. doi: 10.1016/j.compstruct.2018.08.025.
[7] Ferdous W, Manalo A, Alajarmeh OS, Zhuge Y, Mohammed AA, Bai Y, et al. Bending and shear behaviour of waste rubber concrete-filled frp tubes with external flanges. Polymers (Basel) 2021;13. doi: 10.3390/polym13152500.
[8] Chu TB, Gernay T, Dotreppe JC, Franssen JM. Steel hollow columns with an internal profile filled with self-compacting concrete under fire conditions. Proc Roman Acad 2016;17(2):152–9.
[9] Chu TB. Hollow steel section columns filled with self-compacting concrete under ordinary and fire conditions. PhD thesis. University of Liege, Belgium; 2009.
[10] Dotreppe JC, Chu TB, Franssen JM. Steel hollow columns filled with self-compacting concrete under fire conditions. In: 3rd FIB international congress; 2010.
[11] Zhu MC, Meng FQ, He B. Experimental research on fire resistance of steel tubular columns filled with steel reinforced concrete. J Build Struct 2016;37:36–43.
[12] Meng FQ, Zhu MC, Mou B, He B. Residual strength of steel-reinforced concrete-filled square steel tubular (SRCFST) stub columns after exposure to ISO-834 standard fire. Int J Steel Struct 2019;19:850–66. https://doi.org/10.1007/s13296-018-0174-z.
[13] Meng FQ, Zhu MC, Clifton GC, Ukanwa KU, Lim JBP. Performance of square steel-reinforced concrete-filled steel tubular columns subject to non-uniform fire. J Constr Steel Res 2020;166. doi: 10.1016/j.jcsr.2019.105909.
[14] Meng FQ, Zhu MC, Clifton GC, Ukanwa KU, Lim JBP. Fire performance of edge and interior circular steel-reinforced concrete-filled steel tubular stub columns. Steel Compos Struct 2021;41:115–22.
[15] Lie TT. A procedure to calculate fire resistance of structural members. Fire Mater 1984;8(1):40–8.
[16] Dusinberre GM. Heat transfer calculations by finite differences. Scranton, PA: International Textbook Company; 1961.
[17] Lie TT. A method to predict the fire resistance of circular concrete filled hollow steel columns. J Fire Prot Eng 1990;2(4):111–26.
[18] Lie TT. Fire resistance of circular steel columns filled with bar-reinforced concrete. J Struct Eng (ASCE) 1994;120(5):1489–509.
[19] Lie TT, Irwin RJ. Fire resistance of rectangular steel columns filled with bar-reinforced concrete. J Struct Eng (ASCE) 1995;121(5):797–805.
[20] Tan KH, Tang CY. Interaction model for unprotected concrete filled steel columns under standard fire conditions. J Struct Eng (ASCE) 2004;130(9):1405–13.
[21] Wang ZH, Tan KH. Green's function solution for transient heat conduction in concrete-filled CHS subjected to fire. Eng Struct 2006;28(11):1574–85.
[22] Espinos A, Romero ML, Lam D. Fire performance of innovative steel-concrete composite columns using high strength steels. Thin-Walled Struct 2016;106:113–28. https://doi.org/10.1016/j.tws.2016.04.014.
[23] Tan QH, Gardner L, Han LH. Performance of steel-reinforced concrete-filled stainless steel tubular columns at elevated temperature. Int J Struct Stability Dyn 2019;19. doi: 10.1142/S0219455419400029.
[24] Tan QH, Gardner L, Han LH, Song TY. Fire performance of steel reinforced concrete-filled stainless steel tubular (CFSST) columns with square cross-sections. Thin-Walled Struct 2019;143. doi: 10.1016/j.tws.2019.106197.
[25] Mao WJ, Wang WD, Xian W. Numerical analysis on fire performance of steel-reinforced concrete-filled steel tubular columns with square cross-section. Structures 2020;28:1–16. https://doi.org/10.1016/j.istruc.2020.08.043.
[26] Albero V, Espinos A, Romero ML, Hospitaler A, Bihina G, Renaud C. Proposal of a new method in EN1994-1-2 for the fire design of concrete-filled steel tubular columns. Eng Struct 2016;128:237–55. https://doi.org/10.1016/j.engstruct.2016.09.037.
[27] CEN. EN 1994-1-2, Eurocode 4: design of composite steel and concrete structures. Part 1.2: general rules - structural fire design; 2005.
[28] Abaqus/CAE user's guide. Version 2019. Dassault Systèmes; 2019.
[29] CEN. EN 1991-1-2, Eurocode 1: actions on structures - Part 1-2: general actions - actions on structures exposed to fire; 2002.
[30] Ghojel J. Experimental and analytical technique for estimating interface thermal conductance in composite structural elements under simulated fire conditions. Exp Therm Fluid Sci 2004;28:347–54.
[31] Tao Z, Ghannam M. Heat transfer in concrete-filled carbon and stainless steel tubes exposed to fire. Fire Saf J 2013;61:1–11. https://doi.org/10.1016/J.FIRESAF.2013.07.004.
[32] Espinos A, Romero ML, Hospitaler A. Advanced model for predicting the fire response of concrete filled tubular columns. J Constr Steel Res 2010;66(8–9):1030–46. https://doi.org/10.1016/j.jcsr.2010.03.002.
[33] CEN. EN 1993-1-2, Eurocode 3: design of steel structures, Part 1.2: general rules – structural fire design; 2005.
[34] CEN. EN 1992-1-2, Eurocode 2: design of concrete structures, Part 1.2: general rules – structural fire design; 2004.
[35] CEN/TC250/SC2 N1897 - stable version prEN 1992-1-2:2021-09. Eurocode 2: design of concrete structures - Part 1-2: general rules - structural fire design; 2021.
[36] Huang ZF, Tan KH, Phng GH. Axial restraint effects on the fire resistance of composite columns encasing I-section steel. J Constr Steel Res 2007;63:437–47. https://doi.org/10.1016/j.jcsr.2006.07.001.
[37] Huang ZF, Tan KH, Toh WS, Phng GH. Fire resistance of composite columns with embedded I-section steel - effects of section size and load level. J Constr Steel Res 2008;64:312–25. https://doi.org/10.1016/j.jcsr.2007.07.002.

[38] Mao X, Kodur VKR. Fire resistance of concrete encased steel columns under 3- and 4-side standard heating. J Constr Steel Res 2011;67:270–80. https://doi.org/10.1016/j.jcsr.2010.11.006.

[39] Han LH, Tan QH, Song TY. Fire performance of steel reinforced concrete columns. J Struct Eng 2015;141:04014128. https://doi.org/10.1061/(ASCE)ST.1943-541X.0001081.

[40] Du Y, Qi H, Jiang J, Liew JYR, Li S. Thermo-mechanical behaviour of ultra-high strength concrete encased steel columns in standard fires. Eng Struct 2021;231: 111757. https://doi.org/10.1016/j.engstruct.2020.111757.

[41] CEN. EN 1993-1-1, Eurocode 3: design of steel structures - Part 1-1: general rules and rules for buildings; 2005.

[42] CEN/TC250/SC4 N2192 - SC4.T7 Project Team final draft prEN 1994-1-2. Eurocode 4: design of composite steel and concrete structures – Part 1-2: general – structural fire design; 2021.

[43] CEN/TC250/SC4 N1836 - SC4.T4 Final Draft Annex H - simple calculation model for concrete filled hollow sections exposed to fire all around the column according to the standard temperature-time curve; 2017.

[44] Wickström U. A very simple method for estimating temperature in fire exposed concrete structures. Sweden; 1986.